Desalination 586 (2024) 117883

Contents lists available at ScienceDirect

Desalination

journal homepage: www.elsevier.com/locate/desal

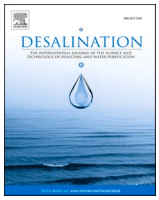

Delithiation and lithiation of $LiFePO_4$: Implications for direct Li extraction from synthetic solutions and geothermal brines

Rebekka Reich *, Elisabeth Eiche, Jochen Kolb

Chair of Geochemistry and Economic Geology, Institute of Applied Geosciences, Karlsruhe Institute of Technology, Adenauerring 20b, 76131 Karlsruhe, Germany
Laboratory for Environmental and Raw Materials Analysis, Institute of Applied Geosciences, Adenauerring 20b, 76131 Karlsruhe, Germany

HIGHLIGHTS

- Chemical and mineralogical characterization of nanocrystalline $LiFePO_4$ powder
- Fast and complete delithiation of $LiFePO_4$ using 0.1 M $Na_2S_2O_8$
- High Li selectivity in geochemically complex fluid compositions
- >99 % Li recovery from geothermal brines

GRAPHICAL ABSTRACT

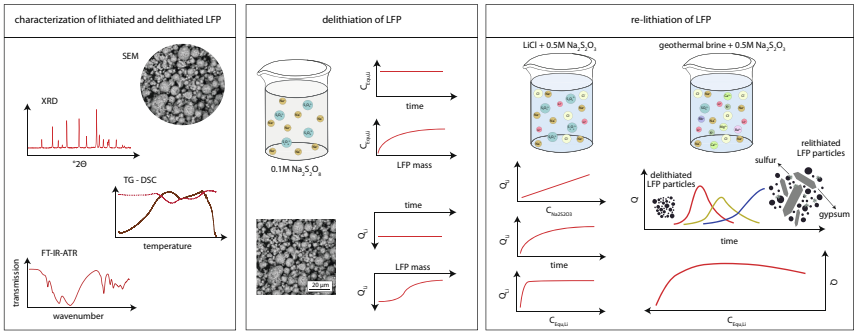

ARTICLE INFO

Keywords:
Lithium iron phosphate
Geothermal brine
Redox additive
Direct lithium extraction (DLE)
Selectivity

ABSTRACT

The demand for Li is and will be increasing in the future, and the development of a direct Li extraction (DLE) technology from unconventional resources, like geothermal brines, may contribute to a resilient supply in the future. This study investigates the deintercalation from and intercalation of Li in $LiFePO_4$ (LFP) at 25–80 °C, near neutral to acidic pH and the effect of high salinity on the Li extraction performance. The (de-)lithiation is a fully reversible redox process between triphylite and heterosite. Lithium is delithiated from LFP using 0.1 M $Na_2S_2O_8$ at 42–43 mg/g. The lithiation kinetics increase with temperature, but show a complex relationship to reducing agent ($Na_2S_2O_3$) concentration. The maximum re-intercalation is achieved in synthetic LiCl + 0.5 M $Na_2S_2O_3$ solution at 39 mg/g, 25 °C and 7 days, whereas 27 mg/g and 1.3 mg/g Li are intercalated to LFP within 3–4 h in experiments with Bruchsal and synthetic Neustadt-Glewe geothermal brines at 60 °C, respectively. At optimal parameters, >99 % Li are recovered from both geothermal brines in laboratory experiments. This shows that LFP can be used for DLE from geothermal brines under specific conditions in a purely chemical process.

* Corresponding author at: Karlsruhe Institute of Technology, Adenauerring 20b, Gebäude 50.40, 76131 Karlsruhe, Germany.
E-mail address: rebekka.reich@kit.edu (R. Reich).

https://doi.org/10.1016/j.desal.2024.117883
Received 25 April 2024; Received in revised form 21 June 2024; Accepted 25 June 2024
Available online 26 June 2024

1. Introduction

Lithium iron phosphate (LFP) is widely used as cathode material in Li-ion batteries in the form of triphylite [1]. LFP batteries are claimed to be eco-friendly, non-toxic, cheap and fulfil higher safety standards than batteries with comparable cathode materials, like $LiCoO_2$ (LCO) or $LiNiMnCoO_2$ (NMC), and are, therefore, expected to replace them in the future [1–3].

The olivine-type $LiFePO_4$ (triphylite) – $FePO_4$ (heterosite) phases are built of FeO_6 octahedra and PO_4 tetrahedra with interstitial Li showing mobility in the *b* direction [2,4–6]. Both phases are orthorhombic in the *Pnma* space group [2,6,7]. In the olivine structure, M1M2TO$_4$ monovalent cations, like Li^+ or Na^+, only occupy the octahedral M1 site whereas divalent cations, like Fe^{2+}, Mg^{2+} or Mn^{2+} occupy the slightly distorted octahedral M2 site [6–8]. The tetrahedral site T is occupied by P, Si or Ge [8].

A miscibility gap between triphylite and heterosite is postulated at temperatures <200 °C [9], becoming smaller with increasing temperature and decreasing grain size [2,10]. The miscibility gap is found for nanoparticle size >15 nm at room temperature and >25 nm at 45 °C, respectively [11]. For macroscopic grains at room temperature, the miscibility gap results in phase compositions of $Li_{1.00–0.05}FePO_4$ triphylite and $Li_{0.00–0.17}FePO_4$ heterosite, respectively [5]. The miscibility gap shrinks, e.g. by doping triphylite with V^{3+}, Mo^{6+}, Ti^{4+}, Al^{3+} or Zr^{4+} [12,13]. The substitution of Fe^{2+} by V^{3+} in the M2 site reduces the Li intercalation capacity because V^{3+} does not participate in the Fe^{+III} – Fe^{+II} redox reaction and remains trivalent in triphylite [12,13]. Lithium diffusion in *b* direction, however, remains unaffected [12,13].

The phase transformation of triphylite to heterosite during delithiation results in a decrease of the unit cell volume by 6.8 % [2]. The unit cell parameters of triphylite are $a = 10.338(1)$ Å, $b = 6.011(1)$ Å and $c = 4.695(1)$ Å [7]. After delithiation, the lattice shrinks at −5.6 % and −4.3 % in the *a* and *b* direction, respectively, whereas it increases in *c* direction by 1.5 % [7]. The resulting heterosite has crystal lattice parameters of $a = 9.760(1)$ Å, $b = 5.752(1)$ Å and $c = 4.756(1)$ Å, and the FeO_6 octahedral site is more distorted than in triphylite [7]. The intercalation of Na in $FePO_4$, however, results in the increase of the unit cell parameters by 16.6 vol% [14]. Oxidation of Fe^{2+} in triphylite may either be accompanied by a vacancy in the M2 site for charge balance ($3Fe^{2+} \rightarrow 2Fe^{3+}$) or in the M1 site (due to lacking substitution of Li) in heterosite [15].

Phase transition between triphylite and heterosite is reversible [15]. The kinetics, however, depend on the Li diffusion along the $LiFePO_4$/$FePO_4$ interface [15]. The mean Fe – O distances vary at a maximum of 0.28 Å after delithiation of triphylite (2.17 Å) to heterosite (2.04 Å) [15]. The reduction of amorphous $FePO_4$, however, is accompanied by the formation of a $Fe_2P_2O_7$ phase which is lacking when crystalline $FePO_4$ is reduced [16].

Calcination of $FePO_4$ at temperatures higher than 300 °C removes the Brønsted acid sites from the surface by evaporation of adsorbed water [16]. As a result, only Lewis acid sites remain [16].

Due to its application as cathode material in Li-ion batteries, the electrochemical properties and the Li recycling potential of LFP are being intensely investigated [e.g., 17,18,19]. The good performance and safety standards of LFP in batteries lead to increasing interest in investigating the electrochemical Li extraction from aqueous solutions using LFP [20,21]. Liu et al. [20] found an average Li^+ capacity of 39 mg/g and a positive correlation between kinetics and applied voltage. A maximum recovery of 91 % is reached after 8 cycles from a brine with 2.5 g/L total dissolved solids (TDS) and 26 mg/L Li [21]. At 1 *V* applied, the Li capacity reaches 11 mg/g, but increases to 17 mg/g by adding polyethylene glycol to the electrode, i.e. a long-chain polymer that increases electrode porosity [21]. The equilibrium time for extraction is 1.5 h [21]. Using a LiCl solution with 220 mg/L Li concentration, the Li capacity reaches 41 mg/g [22]. The presence of Na^+ ions in solution, however, significantly reduces the Li^+ extraction but may be controlled by adjustment of the applied voltage to <0.3 *V* [20]. The selectivity for Li over Mg may be achieved by voltage adjustment to <1 V [22].

Only sparse work has been done addressing the potential application of LFP in direct Li extraction (DLE) from geothermal brines in a purely chemical approach. To extract Li from brines, LFP needs to be delithiated prior to extraction, which can either be achieved by ion exchange or oxidation of Fe^{+II} to Fe^{+III} in the LFP [23,24]. Lithium is isomorphically substituted by Na^+ in a mechanochemical process without using acid [23]. By co-grinding LFP with NaCl, a maximum Li recovery of 12 mg/g is achieved at high $FePO_4$ stability [23]. Lithium is also recovered by Fe oxidation using a solution of 2.4 % H_2O_2 and 0.1 % CH_3COOH, a mixture of H_2O_2 and CO_2, or in a sulfate solution by oxidation of $LiFePO_4$ using $K_2S_2O_8$ or $Na_2S_2O_8$ [19,24–27]. Using a mixture of 1 % H_2O_2 and 3 % CH_3COOH, a complete delithiation is achieved after approximately 400 s using particles of 300 nm diameter [26]. The delithiation kinetics, however, depend on the oxidizing agent concentration, e.g. equilibrium is reached after 20 min using 0.017 M H_2O_2 and after ~15 min using 0.043 M H_2O_2 [19]. Higher oxidation agent concentration increases the delithiation efficiency as well [28]. Using a mixture of 6 % H_2O_2 + 0.8 M CH_3COOH, 94 % Li are recovered at <1 % dissolution of Fe after 60 min [28]. Another significant parameter is the solid-liquid ratio, which should be <100–120 g/L, since higher slurry density decreases the Li elution efficiency [19,28]. Increasing temperature, i.e. 40–60 °C, increases the Li desorption kinetics and capacity, tested for solutions including CH_3COOH and H_2O_2, but behaves inversely if CO_2 is introduced [19,28]. Carbon-coating of LFP has a negligible effect on the delithiation performance [26].

After delithiation of LFP, Fe^{+III} must be reduced during Li extraction. $NaFePO_4$ is successfully synthesized by reduction of heterosite using NaI for 40 h at 60 °C [14]. Complete lithiation of $FePO_4$ was achieved after 300 s at ~60 °C by reduction using 13.4 mmol/L LiI in acetonitrile [25]. Decreasing temperature negatively affects the intercalation of Li, tested in experiments at $T = 7–58$ °C [25]. The lithiation kinetics increase with increasing initial Li concentration and increasing reducing agent concentration [24]. Equilibrium is achieved after 3 h at >0.7 mol/L concentration of both ions in solution at good chemical sorbent stability [24], at least within 50 cycles [25]. A maximum Li uptake of ~46 mg/g $FePO_4$ was achieved by reduction of 0.6–1 g $FePO_4$ with 0.3 M $Na_2S_2O_3$ after 24 h in lithiation experiments with synthetic 0.06–0.2 M LiCl solutions including some competing ions like 2.4–4 M NaCl, 0.2 M KCl or 0.3 M K_2SO_4 and 0.3–1.3 M $MgCl_2$ [24]. The concentration of competing ions sorbed to $FePO_4$ is <3 mg/g after 24 h using 0.3 M $Na_2S_2O_3$ and Li and Na concentrations varying between 0.10 and 0.01 mol/L [24]. A high Li selectivity was also achieved in experiments using a $C_6H_7O_6Na$ reducing agent for DLE from artificial salt lake brine comprising 100 mg/L Li, 82.3 g/L Na, 13.2 g/L Mg and 4.7 g/L K, reaching a maximum Li uptake of 9 mg/g [27]. However, the influence of other (trace) elements on the Li intercalation in LFP for DLE, like Ca, Sr, Ba, B, Pb, As, S, Mn or Zn, usually present at variable concentrations in natural geothermal brines, remains uninvestigated.

Detailed information about quantitative sorbent dissolution and dissolution rates under specific process conditions, the influence of temperature and reaction times >24 h on the extraction process or preferred operating pH, sorption isotherms and underlying sorption processes for Li and competing ions, however, is lacking [24,27]. To directly recover Li from geothermal brines, sorption is regarded as promising technique. Fast sorption and desorption kinetics and a high Li selectivity are indispensable for an efficient extraction process at high ambient flow rates of typically 30–80 L/s and a complex geochemical brine composition [e.g., 29].

In this study, commercially available, carbon-coated LFP cathode material is characterized for its geochemistry and mineralogy. Furthermore, (de-)lithiation kinetics and (de-)lithiation capacity of the nanocrystalline powder are evaluated in a redox process in synthetic $Na_2S_2O_8$ and $Na_2S_2O_3$ + LiCl solutions. The effects of physicochemical parameters, like temperature and pH, on extraction performance and LFP

stability are evaluated. Experiments with pre-precipitated, Fe-depleted natural geothermal brine from the Bruchsal geothermal power plant, operated by EnBW AG, and synthetic geothermal brine similar to the one at Neustadt-Glewe geothermal power plant, operated by Erdwärme Neustadt-Glewe GmbH, in Germany have been conducted to study the material's potential for DLE and its appropriateness regarding stability and Li selectivity.

2. Materials and methods

The Li-Fe-phosphate (IBUvolt® LFP400) was provided by IBU-tec, Weimar, Germany. The samples were investigated optically (SEM), structurally (XRD, TG-DSC, FT-IR-ATR, BET) and chemically (EDX, acid digestion, ICP-OES, ICP-MS). The BSE images and SEM analyses were conducted using a PhenomXL G2 Desktop-SEM from ThermoFisher Scientific at the Department for Petrology and Mineral Resources, Eberhard Karls University Tübingen, Germany.

Two samples that were available at large quantity were analysed by XRD including an internal silicon standard. Therefore, 1.8 g were homogeneously mixed with 0.2 g of standard material and put in sample carriers of 20 mm diameter. The internal silicon standard was introduced to identify texture effects. Samples that were only available at small quantities were attached to a silica wafer with acetone. The XRD analyses were performed with a D8 Discover diffractometer from Bruker with CuKα radiation (Kα1 λ = 1.54060 Å and Kα2 λ = 1.5444 Å) attached to a LYNX-EYE XE-T linear detector at the Laboratory for Environmental and Raw Materials Analyses (LERA), Karlsruhe Institute of Technology, Germany. The conditions were 2–82°2Θ, 1 s/step and 0.02° increment. The sample rotation was 30 rpm, the airscatter was on automatic mode and the X-ray tube operated at 40 kV and 40 mA. The software package Bruker Diffrac.EVA V4.1.1 and the database PDF2 of 2002 were used for phase identification [30].

For the 5-point-BET method with N_2 ($0.05 < p/p0 < 0.35$), the LFP powder was dried at 105 °C under vacuum overnight. Subsequently, the specific surface area (SSA) was determined with a Quantachrome NOVA 4000e instrument at the Institute for Technical Chemistry, Karlsruhe Institute of Technology, Germany. An external Al_2O_3 standard (SSA = 5.1 m^2/g) was used for quality control and the analytical uncertainty was determined to 4 %.

FT-IR-ATR analyses were conducted using a Nicolet iS50 instrument at the Institute of Nanotechnology, Karlsruhe Institute of Technology, Germany. Analyses were performed at wavenumbers between 400 cm^{-1} and 4000 cm^{-1} at contact with a diamond crystal. Each sample was measured using 20 repetitions that were referenced to a background analysis in air.

The phase stability was investigated by TG-DSC analysis with a sintered corundum standard reference material. The powder was filled in a ceramic crucible and heated to 1000 °C in a N_2 atmosphere using a STA 409 PC Luxx system from Netzsch at the LERA. The measurement started at room temperature, followed by heating to 30 °C (heating rate of 10 K/min) which was kept for 10 min. Thereafter, heating to 1000 °C was carried out at 5 K/min. After reaching the maximum temperature, the analysis was stopped.

A sorbent mass of 0.1 g LFP was digested in 2.5 mL 65 % HNO_3 (suprapur®), 0.6 mL 30 % HCl (suprapur®, Merck) and 2.5 mL millipore water. The samples were digested using a Multiwave 5000 instrument from Anton Paar Germany GmbH with a 20SVT50 rotor. The temperature was increased to 100 °C within 5 min. Afterward, the system was heated to 230 °C within 25 min and held for 15 min. After cooling to room temperature, the solution was diluted in millipore water to a total volume of 50 mL.

All solutions (from experiments and digestions) were analysed with an ICP-OES (iCAP 7000, Thermo Fisher) at LERA. The solutions from the acid digestion of sample material from the experiments with geothermal brine were additionally analysed for trace element content using an ICP-MS iCAP RQ (C2) with an iMR_1000 gas kit (Thermo Fisher) at LERA. Lithium, Na, P, S and Fe were analysed in all solutions. The samples related to experiments with geothermal brines were additionally analysed for K, Rb, Cs, Mg, Ca, Sr, Ba, B, Al, Si, Pb, As, Sb, Ti, *V*, Cr, Mn, Co, Ni, Cu, Zn, and Cd. Solutions containing $Na_2S_2O_3$ additive cause analytical difficulties since they cannot be analysed in an 1 % HNO_3 matrix due to acid sensitivity of $Na_2S_2O_3$. The analyses have been performed in millipore water, which leads to potential underestimation of metal concentrations, like As, Pb and Fe. Duplicates and certified standards (e.g., a multi-element aqueous VHG-MISA6–500 standard, a high-purity multi-element standard CRM-TMDW-A for trace metals in drinking water, and an internal standard ROTI®Star 1000 mg/L Y in 2 % HNO_3 for diluted samples) were analysed for quality control and estimation of the analytical uncertainty. Additionally, blanks were analysed to determine the detection limit (LOD, 3 times sigma) and the limit of quantification (LOQ, 10 times sigma; supplementary data).

The (de-)lithiation capacity is calculated using the equation $Q_i = \left(C_0 - C_{Equ}\right) * \frac{V}{m}$. Q is the amount of sorbate (i) in the sorbent in mg/g (when different sorbates are compared, the value is recalculated to mmol/g), C_0 is the initial concentration of the sorbate in the solution in mg/L, C_{Equ} is the equilibrium concentration of the sorbate in the solution after the experiment in mg/L, *V* is the volume of the solution in L and m is the sorbent mass in g used in the experiment or the digestion [31].

2.1. Experimental

The batch (de-)lithiation experiments were performed after the procedure described in Reich et al. [32]. In initial delithiation experiments, 1 g LFP and 200 mL of different solutions in variable concentrations (e.g. 0.01–0.50 M HCl (pro analysis, Merck), 0.1–3.0 M NaCl (pro analysis, Merck), mixtures of H_2O_2 (pro analysis, Roth) and CH_3COOH (pro analysis, Merck) and 0.1–1.0 M $Na_2S_2O_8$ (normapur™, VWR)) were used. The experiments were stirred for 45 min and 24 h (for HCl). Best performance was reached for a 0.1 M $Na_2S_2O_8$ solution, which was used with the same sorbent/fluid ratio at variable stirring time (delithiation kinetics), and a variable sorbent/fluid ratio at a fixed stirring time of 60 min (delithiation isotherm).

For the lithiation experiments, variable concentrations of 0.1–1.5 M $Na_2S_2O_3$ (pro analysis, Merck) were used with a fixed sorbent/fluid ratio (1 g/200 mL) and Li concentration (200 mg/L) in synthetic LiCl – $Na_2S_2O_3$ solutions. A 0.5 M $Na_2S_2O_3$ matrix was used, which is advantageous for ICP-OES analyses since higher $Na_2S_2O_3$ concentration would require higher dilution of samples, making trace element analysis challenging. The kinetic experiments with synthetic solutions were conducted at 25 °C and a Li concentration of 200 mg/L. The stirring time varied between 1 min and 2 weeks. For the lithiation isotherm experiments in synthetic LiCl solution, the Li concentration was varied between 10 and 1000 mg/L and the stirring time was seven days. Experimental batches have been performed at 25, 40, 60 and 80 °C to study the temperature influence.

All experiments with geothermal brine were conducted at 60 °C. In kinetic experiments, the stirring time was varied between 1 min and 2 weeks. A constant stirring rate of ~300 rpm was used in Bruchsal brine experiments. The experiments with synthetic geothermal brine (Neustadt-Glewe) were shaken. The sorbent mass was varied in the isotherm experiments (between 0.2 and 75 g/L) that were stirred for 3 h and 4 h using geothermal brine from Bruchsal and the synthetic geothermal brine of Neustadt-Glewe composition, respectively. For quality control, blank experiments were conducted in each experimental run.

3. Results

3.1. Material characterization

Both, LFP cathode material (initial $LiFePO_4$) and its delithiated form ($FePO_4$) are used as starting material in the experiments. The initial

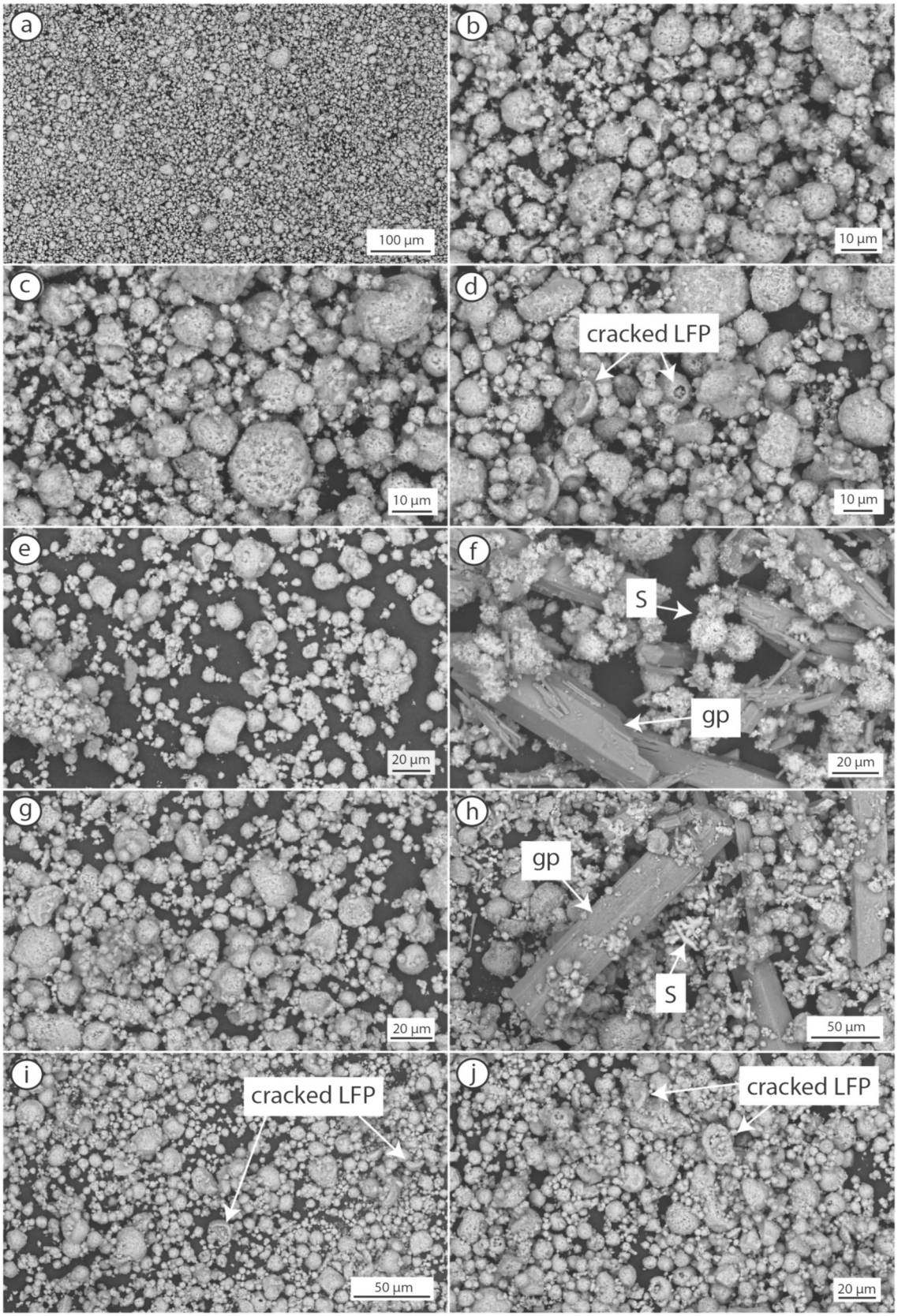

Fig. 1. BSE images of LFP samples. a) and b) initial $LiFePO_4$ powder, c) $FePO_4$ sample after delithiation using 0.1 M $Na_2S_2O_8$, d) sample after synthetic LiCl + $Na_2S_2O_3$ solution treatment, e) sample after geothermal brine + $Na_2S_2O_3$ treatment (1 g, 3 h, Bruchsal), f) sample after two weeks reaction time with geothermal brine + $Na_2S_2O_3$ (Bruchsal), g) sample after 4 h reaction time with synthetic brine + $Na_2S_2O_3$ (Neustadt-Glewe), h) sample after one week reaction time with synthetic brine + $Na_2S_2O_3$ (Neustadt-Glewe), i) sample after brine + $Na_2S_2O_3$ treatment (5 g, 3 h, Bruchsal) and j) sample after brine + $Na_2S_2O_3$ treatment (10 g, 3 h, Bruchsal).

Table 1
Chemical composition of initial $LiFePO_4$ starting material and $FePO_4$.

	$LiFePO_4$ [mg/g]	$FePO_4$ [mg/g]
Li	43	1.7
Fe	266	247
P	161	145
Na	<0.3	0.98
K	0.09	<0.05
Mg	0.11	0.12
Al	0.08	0.07
Si	0.05	0.08
S	0.86	1.02
Ti	0.02	0.02
Mn	0.46	0.42
Co	0.05	0.05
Ni	0.06	0.07
Cu	0.10	0.10
Zn	0.06	0.07
Rb	<0.0005	<0.0005
Cs	<0.0005	<0.0005
Ca	<0.1	<0.1
Sr	<0.0002	<0.0002
Ba	<0.0003	<0.0003
B	<0.005	<0.005
Pb	<0.0005	<0.0005
As	<0.01	<0.01
Sb	<0.0005	<0.0005
V	<0.003	<0.003
Cr	<0.006	0.01
Cd	<0.0009	<0.0009

$LiFePO_4$ is composed of rounded nanoparticles that appear homogeneous with a grain size ranging between approximately 1–20 μm (Fig. 1a). A distinct micro porosity is visible on the surface of each particle (Fig. 1b). The initial $LiFePO_4$ has a specific surface area of 21.5 m^2/g. Its Li content is 43 mg/g (Table 1).

Iron and P concentrations are 266 mg/g and 161 mg/g, respectively. The $FePO_4$, in contrast, contains 1.7 mg/g Li, 247 mg/g Fe and 145 mg/g P (Table 1). The mineral formulae for $LiFePO_4$ and $FePO_4$ are approximately $Li_{1.000}Fe_{0.996}Mg_{0.001}Mn_{0.002}PO_4$ and $Li_{0.051}Na_{0.009}Fe_{0.936}Mg_{0.001}Mn_{0.002}PO_4$, respectively. The XRD data confirm that the initial $LiFePO_4$ is well crystalline and identifies it as orthorhombic triphylite endmember (Fig. 2I.). The $FePO_4$ is the orthorhombic heterosite endmember (Fig. 2II.).

TG-DSC data show minor mass variation (±3 %) between 30 and 1000 °C in $LiFePO_4$, whereas $FePO_4$ loses 10 % total mass by heating to 1000 °C with strongest mass loss (~8 %) starting at approximately 530 °C (Fig. 3a). The $LiFePO_4$ shows, after an initial mass loss of ~2 %, a two-step mass increase starting at ~550 °C (Fig. 3a). The DSC curve of the $LiFePO_4$ shows an endothermic peak at 55 °C (−0.04 mW/mg), and three exothermic peaks at 538 °C (+1.51 mW/mg), 652 °C (+1.25 mW/mg) and 863 °C (+1.56 mW/mg), respectively. The $FePO_4$ sample shows a similar DSC curve with an endothermic peak at 58 °C (−0.05 mW/mg) and two sharp exothermic peaks at 573 °C (+1.31 mW/mg) and 654 °C (+1.25 mW/mg), respectively.

The FT-IR-ATR spectra of the $LiFePO_4$ sample have characteristic bands at 460 cm^{-1}, 496 cm^{-1}, 545 cm^{-1}, 574 cm^{-1}, 633 cm^{-1}, 927 cm^{-1}, 1030 cm^{-1}, 1138 cm^{-1}, 1205 cm^{-1} and 3430 cm^{-1}, respectively (Fig. 4).

3.2. Delithiation

Different solutions have been tested for delithiation of $LiFePO_4$ to produce $FePO_4$ that is needed for the DLE process. Delithiation can either be performed by Fe oxidation or by ion-exchange. Different oxidizing solutions, like 1 % H_2O_2 + 3 % CH_3COOH [26], 2.4 % H_2O_2 + 0.1 % CH_3COOH [25], 0.1 % H_2O_2 + 1 % CH_3COOH and 0.1 M, 0.5 M and 1.0 M $Na_2S_2O_8$ are tested. For delithiation by ion exchange, 0.1–3.0 M NaCl and 0.01–0.50 M HCl are used. The efficiency of delithiation and the elution of Fe and P are checked by determining the amount of each element eluted from $LiFePO_4$ by the respective solution.

A small amount of Li (1–3 mg/g) and P (5–7 mg/g) are rinsed from $LiFePO_4$ in blank experiments using millipore water (Fig. 5). Using different mixtures of H_2O_2 + CH_3COOH (i.e., oxidation agents), 81–99 % of Li is eluted (5.02–6.14 mmol/g; 35–43 mg/g) (Fig. 5). Phosphorous and Fe are eluted at 0.2–0.3 mmol/g (7–9 mg/g) and 0.003–0.03 mmol/g (0.2–2.0 mg/g), respectively, only slightly more than using millipore water. The Li elution is less variable using 0.1–1.0 M $Na_2S_2O_8$ solutions: 96–99 % (5.98–6.14 mmol/g; 41–43 mg/g) Li are recovered from $LiFePO_4$ powder, whereas Fe and P loss are low at <0.01 mmol/g (<0.4 mg/g) and 0.22 mmol/g (<7 mg/g), respectively (Fig. 5). With 0.1–3.0 M NaCl, Li, Fe and P are eluted at 0.14–0.25 mmol/g (1–2 mg/g), <0.001 mmol/g (<0.05 mg/g) and 0.10–0.18 mmol/g (3–6 mg/g), respectively. In contrast, 36–98 % (15–42 mg/g) Li, 0–100 % Fe and 6–100 % P are eluted using 0.01–0.50 M HCl (Fig. 5).

The delithiation kinetics is investigated using a 0.1 M $Na_2S_2O_8$ solution. Equilibrium is reached within 1 min reaction time and the delithiation capacity reaches 42–43 mg/g (Figs. 6a, 7a, b) at low Fe and P loss (1–2 mg/g and 5–7 mg/g, respectively). The starting pH is 3.1–3.6 in both, kinetic and isotherm delithiation experiments. The pH increases to 5.3 within 5 min and decreases exponentially to 2.3 after 2 weeks reaction time (Fig. 6b).

The maximum concentration of Li in the delithiation solution after the reaction is approximately 1.5 g/L Li at an optimal $LiFePO_4$/fluid ratio of <35 g/L (Fig. 7a, b). At higher $LiFePO_4$/fluid ratios, the Li concentration in the solution only slightly increases but the $LiFePO_4$ is not fully delithiated (Fig. 7a, b). At $LiFePO_4$/fluid ratios <0.5 g/L, the Fe and P loss are highest, at maximum 0.07–0.09 mmol/g (4–5 mg/g) and 0.23–0.26 mmol/g (7–8 mg/g), respectively. Sodium and S are sorbed to $LiFePO_4$ at 0.03–0.10 mmol/g (0.6–2.0 mg/g) and 0.01–0.08 mmol/g (0.2–3.0 mg/g), respectively (Fig. 7a, b). The pH increases with higher $LiFePO_4$/fluid ratios to pH = 8, with an increase in slope at a $LiFePO_4$/fluid ratio of 25 g/L and pH = 3.9 (Fig. 7c).

The delithiation of $LiFePO_4$ using a 0.1 M $Na_2S_2O_8$ solution does not change the particle shape at micro scale (Fig. 1c). The round grains and the micro porosity seem unchanged compared to the initial $LiFePO_4$ sample (Fig. 1b, c). However, structural changes are identified by XRD and FT-IR-ATR (Figs. 2II., 4). An orthorhombic heterosite phase is identified but the specific reflexes that are expected at 30.64°2Θ, 40.68°2Θ, 54.29°2Θ are shifted to 30.90°2Θ, 40.79°2Θ, 54.56°2Θ, respectively. An additional reflex at 64.35°2Θ occurs in the pattern that is not identified (Fig. 2II.). The bands in the FT-IR-ATR spectrum that were identified at 1030 cm^{-1}, 927 cm^{-1} and 633 cm^{-1} are shifted to 1067 cm^{-1}, 902 cm^{-1} and 646 cm^{-1}, respectively. An additional band at 514 cm^{-1} is identified. The tiny band, initially present at 1205 cm^{-1}, became a strong band at 1238 cm^{-1} (Fig. 4).

3.3. Lithiation experiments with pure LiCl – $Na_2S_2O_3$ solution

In lithiation experiments using a solution of 200 mg/L LiCl and 0.1–1.5 M $Na_2S_2O_3$, the sorption of Li shows a near-linear behaviour correlating positively with the $Na_2S_2O_3$ concentration (Fig. 8a). The Li sorption capacity in mg/g and mmol/g, i.e. the intercalated amount of Li in $FePO_4$ within 24 h, are estimated as a function of additive concentration:

$$Q_{Li}\left[\frac{mg}{g}\right] = 15.093 * c(Na_2S_2O_3)\left[\frac{mol}{L}\right] - 0.6282, \text{ or} \quad \text{(F.1)}$$

$$Q_{Li}\left[\frac{mmol}{g}\right] = 2.1745 * c(Na_2S_2O_3)\left[\frac{mol}{L}\right] - 0.0905. \quad \text{(F.2)}$$

At 1.5 M $Na_2S_2O_3$, the Li sorption capacity reaches 3 mmol/g (21 mg/g), whereas only 0.04 mmol/g (0.3 mg/g) Li are sorbed to $FePO_4$ using 0.1 M $Na_2S_2O_3$ (Fig. 8a). Sulfur and Na sorption capacities increase

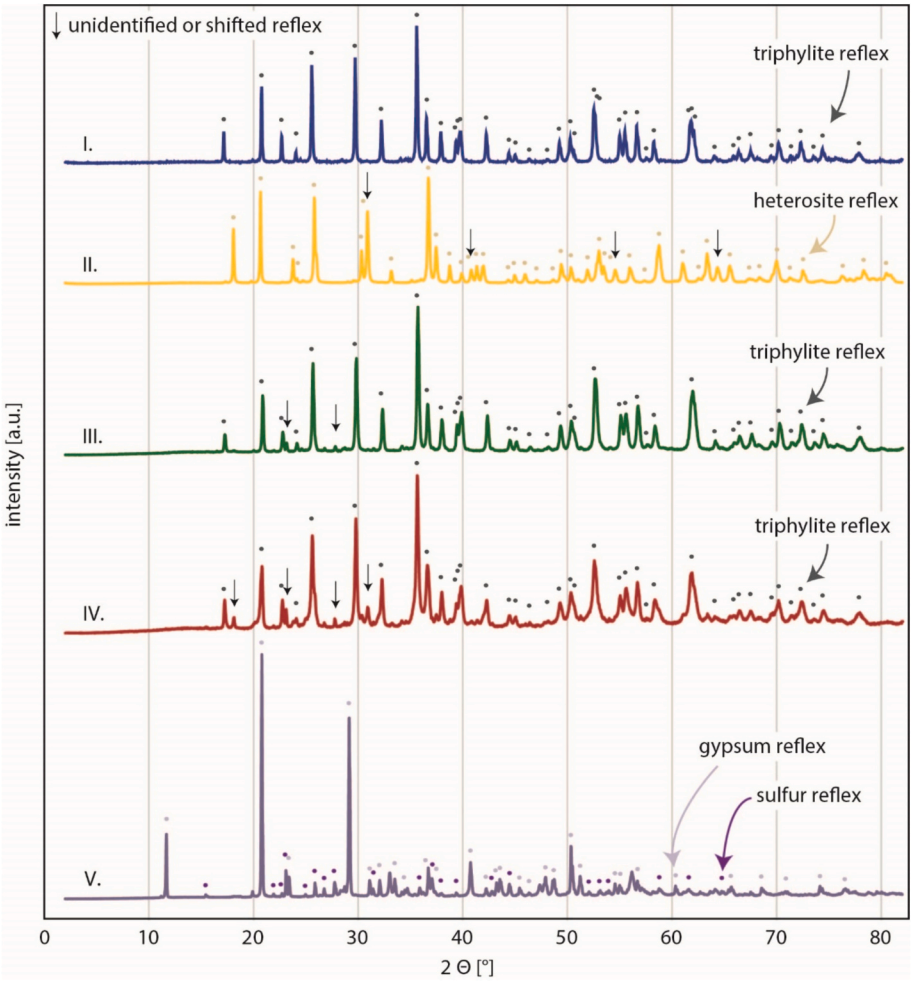

Fig. 2. XRD patterns. Reflexes of the identified phase are highlighted by dots. Arrows highlight reflexes that could not be related to the identified phases or shifts of single reflexes compared to the initial $LiFePO_4$ material. I.) orthorhombic triphylite initial material, II.) orthorhombic heterosite after delithiation, III.) orthorhombic triphylite re-lithiated by LiCl +0.5 M $Na_2S_2O_3$ solution (25 °C, 7 days, 5 g/L $FePO_4$, 1000 mg/L initial Li concentration), *IV.*) orthorhombic triphylite re-lithiated by geothermal brine +0.5 M $Na_2S_2O_3$ (60 °C, 3 h, 5 g/L $FePO_4$, 160 mg/L initial Li concentration) and *V.*) gypsum and native sulfur in LFP sample after two weeks reaction time with Bruchsal geothermal brine +0.5 M $Na_2S_2O_3$ (60 °C, 2 weeks, 5 g/L $FePO_4$, 160 mg/L initial Li concentration).

with increasing $Na_2S_2O_3$ concentration, reaching 0.8 mmol/g (26 mg/g) and 0.9 mmol/g (20 mg/g) at maximum, respectively (Fig. 8a).

After seven days reaction time at 25 °C using a 0.5 M $Na_2S_2O_3$ matrix, Li sorption reaches equilibrium (Fig. 8b). The maximum Li sorption capacity is at 6.35 mmol/g (44 mg/g), which corresponds to 100 % lithiation within analytical uncertainty. The elution of Fe and P is below detection limit at reaction times shorter than 24 h. At longer reaction times, elution of Fe and P starts and is at maximum after two weeks (0.63 mmol/g (35 mg/g) Fe and 0.71 mmol/g (22 mg/g) P). Sodium sorption is not detected during the first two days reaction time, but reaches a maximum of 0.34 mmol/g (8 mg/g) after two weeks. Sulfur sorption is observed within the first five minutes, at 0.004 mmol/g (0.1 mg/g), increasing to 2.58 mmol/g (83 mg/g) after two weeks (Fig. 8b). The starting pH in experiments with 0.5 M $Na_2S_2O_3$ matrix is 9.0–9.4. After 1 min – 5 days reaction time, the pH varies between 6.8 and 7.7 (Fig. 8b). A reaction time of 5 days – 2 weeks leads to a pH decrease to 5.5 and elution of P starts. The P and Fe elution reaches its maximum at the lowest pH (Fig. 8b). Maximum Li sorption capacity is reached at 25 °C with 39 mg/g, whereas only 31 mg/g is sorbed to $FePO_4$ at 40 °C and no Li sorption was detectable at 60 and 80 °C (Fig. 8c).

Lithiation of $FePO_4$ does not affect the particles at micro-scale, except of few cracks (Fig. 1d). Two minor additional reflexes at 23.14°2Θ and 27.79°2Θ are visible in the XRD pattern, not related to triphylite (Fig. 2III.). The re-lithiated $FePO_4$ shows the same FT-IR-ATR bands as the initial $LiFePO_4$ sample (Fig. 4), with only a minor shift of the bands at 1030 cm^{-1} and 927 cm^{-1} to 1040 cm^{-1}, 937 cm^{-1}.

3.4. Lithiation kinetics with geothermal brine and $Na_2S_2O_3$ additive

The Neustadt-Glewe geothermal brine has significantly lower concentrations of Li, K, B, SiO_2 and As than the Bruchsal geothermal brine, i.e. 11 mg/L vs. 155 mg/L Li, 830 mg/L vs. 3240 mg/L K, 0.05 mg/L vs. 41 mg/L B, 32 mg/L vs. 90 mg/L $SiO_{2(aq)}$ and <0.0001 mg/L vs. 7.8 mg/L As (Table 2). The Na and Mg concentrations, however, are higher in the Neustadt-Glewe brine than in the Bruchsal geothermal brine (74,700 mg/L vs. 35,600 mg/L and 1320 mg/L vs. 340 mg/L, respectively; Table 2).

3.4.1. Bruchsal geothermal brine

The Li sorption increases quickly in kinetic experiments at short reaction times using Bruchsal geothermal brine, reaching a maximum and thereafter, the Li sorption slowly decreases at longer reaction times (Fig. 9a). Maximum Li sorption of 23 mg/g (3.37 mmol/g) is reached after 3 h. Lithiation does not affect the material at micro-scale until the maximum sorption capacity is reached (Fig. 1e). The XRD data confirm the formation of orthorhombic $LiFePO_4$ after lithiation (Fig. 2IV.). Additional reflexes are identified at 18.10°2Θ, 23.10°2Θ, 27.73°2Θ and 30.89°2Θ that cannot be related to a coexisting heterosite phase. The FT-

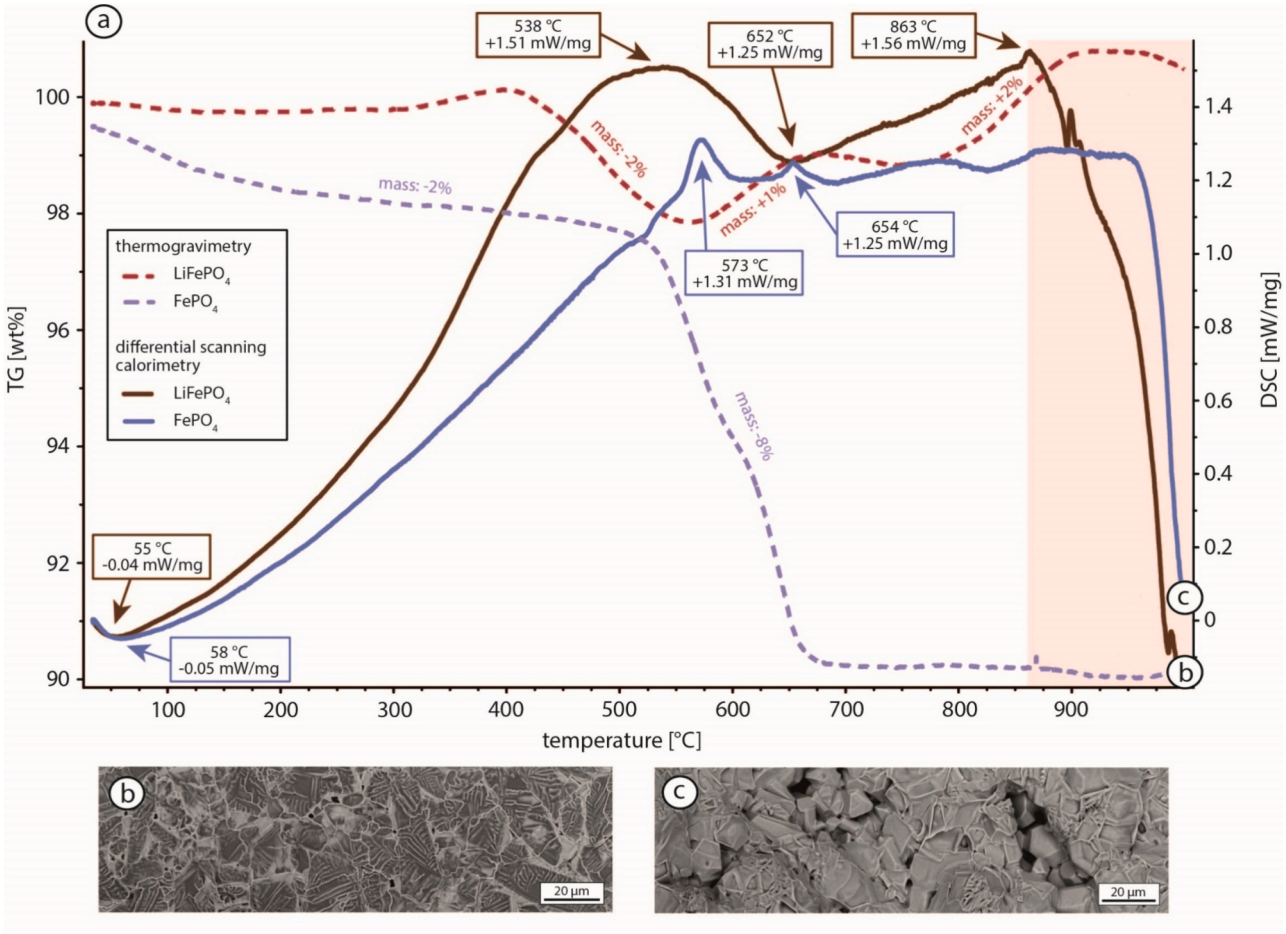

Fig. 3. a) TG-DSC results for $LiFePO_4$ and $FePO_4$. The mass change [wt%] during heating is illustrated by dashed lines, whereas the solid lines reflect the DSC results [mW/mg] during heating. b) BSE image of crystallized $LiFePO_4$ melt and c) BSE image of crystallized $FePO_4$ melt.

IR-ATR spectrum is similar to the initial $LiFePO_4$ and the $FePO_4$ sample re-lithiated from the synthetic $LiCl + Na_2S_2O_3$ solution (Fig. 4). Only the band at 927 cm^{-1} shows a shift beyond the analytical uncertainty to 934 cm^{-1}.

Sodium shows a similar behaviour as Li, but the maximum Na sorption capacity is reached later (after 24 h) (Fig. 9a). The elution of Fe and P is low until the maximum Li sorption capacity is reached and increases to −123 mg/g (−2.2 mmol/g) Fe after 3 days reaction time and −114 mg/g (−3.7 mmol/g) P loss after one week reaction time (Fig. 9a). The starting pH is 6.9–7.3. It decreases exponentially with stirring time, until equilibrium is reached at pH = 3.7–4.1 after 24 h (Fig. 10).

Sorption of S and Ca increases with reaction time and is at maximum with 10.7 mmol/g (344 mg/g) S and 3.8 mmol/g (154 mg/g) Ca after 2 weeks (Fig. 9a). Strong increase in S and Ca sorption correlates with the decrease in Fe elution. In BSE images, elongated, euhedral crystals are observed after long stirring time (Fig. 1f) and the surface of the LFP particles is rough (Fig. 1b, f).

At short reaction time, Sr is already sorbed to $FePO_4$ with 0.003–0.007 mmol/g (0.2–0.6 mg/g) and reaches maximum at 0.02 mmol/g (1.4 mg/g) after 3 days. Sorption of Ba is generally low, at 0.001 mmol/g (0.05–0.08 mg/g) at the start and increases to 0.002 mmol/g (0.2 mg/g) after 1–3 days. The sorption of both elements is low until Fe and P elution starts (Fig. 9a).

Sorption of other elements reaches maximum values of 0.004–0.015 mmol/g (0.1–0.6 mg/g) for K and 0.002 mmol/g (0.10 mg/g) for Mg. At maximum, As sorption is 0.004 mmol/g (0.3 mg/g) after 5 days. The sorption kinetics of Mn, Si, Zn and Pb are inconclusive (Fig. 9a). In general, however, the sorption capacities are low. Zink and Pb are extracted from the brine with a maximum of 0.005 mmol/g (0.3 mg/g) and 0.0001 mmol/g (0.01 mg/g), respectively. Manganese is partially eluted from $FePO_4$, but also shows positive sorption values depending on the reaction times and varies between −0.006–0.001 mmol/g (−0.3–0.1 mg/g). Silica shows low elution from $FePO_4$ at −0.003 mmol/g (−0.08 mg/g).

3.4.2. *Synthetic Neustadt-Glewe geothermal brine*

The kinetics is similar to the results for the Bruchsal brine, but Li sorption is at maximum after 4 h (Fig. 9b). Sodium shows a similar behaviour as Li and reaches the maximum sorption capacity after 24 h, i. e. the same as observed for the Bruchsal brine. The Fe and P elution is at maximum at −98 mg/g (−1.7 mmol/g) after 3 days and −65 mg/g (−2.1 mmol/g) after 5 days, respectively (Fig. 9b). The starting pH is 7.0–7.7. The pH decreases with time, reaching an equilibrium pH = 3.8–4.0 after 24 h (Fig. 10).

Sorption of S and Ca increases with long reaction times and is at maximum with 8.3 mmol/g (265 mg/g) S and 3.5 mmol/g (139 mg/g) Ca after 2 weeks (Fig. 9b). As already observed in the Bruchsal kinetic experiments (Section 3.4.1), short reaction times do not affect the $FePO_4$ particles at micro-scale (Fig. 1g), but elongated, euhedral crystals form after long stirring time (Fig. 1h) and the surface of the LFP particles is rough (Fig. 1b, h).

Strontium is sorbed at the start of the experiment with 0.002–0.005 mmol/g (0.2–0.4 mg/g) and reaches maximum at 0.01 mmol/g (1.2 mg/g) after 3 days. Barium is generally low at the start, with 0.001 mmol/g (0.03–0.08 mg/g), and increases to 0.002 mmol/g (0.1–0.3 mg/g) after

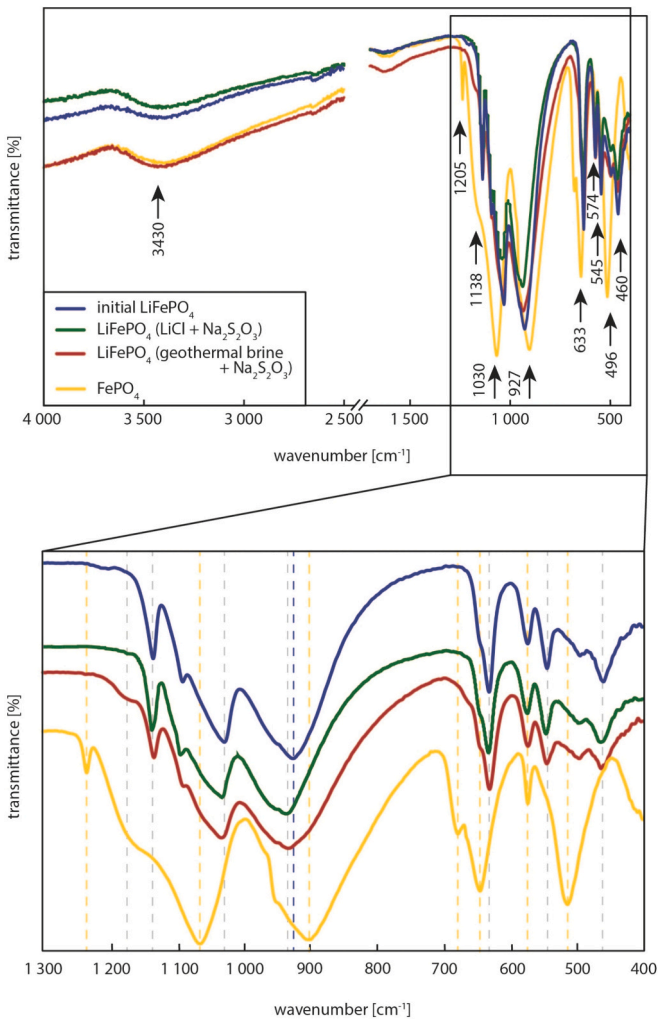

Fig. 4. FT-IR-ATR spectra in the range of 400–4000 cm^{-1} of initial $LiFePO_4$ (blue), $FePO_4$ (yellow), re-lithiated sample using LiCl +0.5 M $Na_2S_2O_3$ solution (green; 25 °C, 7 days, 5 g/L $FePO_4$, 1000 mg/L initial Li concentration) and re-lithiated sample using Bruchsal geothermal brine (red; 60 °C, 3 h, 5 g/L $FePO_4$, 160 mg/L initial Li concentration). The identified bands for the initial $LiFePO_4$ sample are labelled in the upper graph. The dashed lines in the lower graph highlight the shift of characteristic bands in the range of 400–1300 cm^{-1}.

1–3 days. The sorption behaviour of Sr and Ba is the same as already observed in experiments with Bruchsal brine (Section 3.4.1).

Sorption reaches maximum values of 0.003 mmol/g (0.1 mg/g) for K and 0.01 mmol/g (0.3 mg/g) for Mg. The kinetics of Mn, Si, Zn and Pb are inconclusive and behave differently than observed in the kinetic experiments with Bruchsal brine (Fig. 9). In general, however, the sorption capacities are low. Zink and Pb are extracted from the brine with a maximum of 0.001 mmol/g (0.1 mg/g) and 0.001 mmol/g (0.1 mg/g), respectively. Manganese is partially eluted from $FePO_4$, but also shows positive sorption values depending on the reaction time and varies between −0.003–0.001 mmol/g (−0.2–0.2 mg/g).

3.5. Lithiation isotherms with geothermal brine and $Na_2S_2O_3$ additive

3.5.1. Bruchsal geothermal brine

The isotherm shows a typical Langmuir behaviour, with increasing Li sorption capacity at increasing residual Li concentration. At residual Li concentrations >80 mg/L, however, the Li sorption decreases (Fig. 11a). The maximum Li sorption capacity reaches 3.9 mmol/g (27 mg/g). After the strong increase, the Li sorption decreases at $FePO_4$/brine ratios >2.5 g/L (Fig. 11b). The equilibrium Li concentration at $FePO_4$/brine ratios >25 g/L is below the detection limit. A maximum Na sorption of 4.7 mmol/g (107 mg/g) is reached at the smallest tested $FePO_4$/brine ratio of 0.25 g/L. Sorption of S reaches maximum of 1.8 mmol/g (58 mg/g) at a $FePO_4$/brine ratio of 0.25 g/L and decreases with increasing $FePO_4$/brine ratios (Fig. 11b).

Calcium, Sr, Mg, Mn, Si, As, Zn and B show a similar sorption behaviour, reaching high sorption capacities at an $FePO_4$/brine ratio of 0.25 g/L and a decreasing capacity at higher $FePO_4$/brine ratios (Fig. 11b). The maximum capacities are 0.3 mmol/g (14 mg/g) Ca, 0.009 mmol/g (0.8 mg/g) Sr, 0.03 mmol/g (0.6 mg/g) Mg, 0.001 mmol/g (0.1 mg/g) Mn, 0.01 mmol/g (0.3 mg/g) Si, 0.005 mmol/g (0.3 mg/g) As, 0.02 mmol/g (1.4 mg/g) Zn and 0.04 mmol/g (0.5 mg/g) B. The sorption capacities of K and Ba are low at small $FePO_4$/brine ratios <5 g/L, before reaching equilibrium at $FePO_4$/brine ratios >5 g/L at approximately 0.01 mmol/g (0.4 mg/g) K and 0.001 mmol/g (0.13 mg/g) Ba (Fig. 11b). The elution of Fe and P is not continuous, reaching a maximum at −0.04 mmol/g (−2 mg/g) and −0.03 mmol/g (−1 mg/g), respectively.

In the Bruchsal isotherm experiments, the pH value progressively decreases with increasing Li extraction to pH = 3.6. The pH decreases exponentially with increasing $FePO_4$/brine ratio, reaching equilibrium at $FePO_4$/brine ratios >25 g/L and pH = 3.6–3.9 (Fig. 10).

3.5.2. Synthetic Neustadt-Glewe geothermal brine

The lithiation isotherm from the Neustadt-Glewe brine is different compared to the Bruchsal brine experiments (Fig. 11a, c). No typical sorption behaviour, as described by Henry, Langmuir or BET can be identified and the sorption capacities are relatively constant with increasing residual Li concentration (Fig. 11c). The total Li sorption is lower due to the lower initial Li concentration (Table 2, Fig. 11a, c). The maximum Li sorption capacity is 0.2 mmol/g (1.3 mg/g) at an $FePO_4$/brine ratio of 2 g/L (Fig. 11d). Sodium shows the opposite behaviour but not as distinctly as observed in the Bruchsal isotherm (Fig. 11b, d). The maximum Na sorption capacity is 1.7 mmol/g (38 mg/g) at an $FePO_4$/brine ratio of 8 g/L. A typical L isotherm shape is observed for S, reaching a mean equilibrium sorption capacity of 0.4 mmol/g (14 mg/g) at 8–60 g/L. The capacities of Ca, Mg, Zn and Pb decrease after the initial maximum at 0.2 g/L $FePO_4$/brine ratio at 0.1 mmol/g (4.4 mg/g), 0.02 mmol/g (0.4 mg/g), 0.01 mmol/g (0.9 mg/g) and 0.01 mmol/g (1.7 mg/g), respectively (Fig. 11d). The elution of Fe and P are higher in the Neustadt-Glewe than in the Bruchsal experiments and the mean dissolution rates at −0.09 mmol/g (−5.2 mg/g) Fe elution and −0.07 mmol/g (−2.2 mg/g) P elution stay constant over all tested $FePO_4$/brine ratios >8 g/L. The pH progressively decreases with progressing Li extraction to 3.6 and exponentially decreases with increasing $FePO_4$/brine ratio, reaching the equilibrium at $FePO_4$/brine ratios >16 g/L and pH = 3.6–3.9 (Fig. 10).

3.6. LFP selectivity

No robust distribution coefficients (K_d) for the different elements can be calculated because the isotherms do not fit known sorption models, like Henry, Langmuir or BET. Distribution coefficients, however, can be calculated for different points of the isotherms by Eq. (F.3) [31]. The calculated distribution coefficients are thus only valid for the specific conditions under which the experiments have been performed.

$$K_d \left[\frac{L}{g}\right] = \frac{Q_{Equ}\left[\frac{mg}{g}\right]}{C_{Equ}\left[\frac{mg}{L}\right]} \tag{F.3}$$

Different distribution coefficients are calculated for the lithiation peak in kinetic experiments with Bruchsal geothermal brine (Fig. 12a; Table 3), the maximum Li sorption capacity in isotherm experiments from Bruchsal geothermal brine (Fig. 12b; Table 3), the peak lithiation in kinetic experiments from synthetic Neustadt-Glewe geothermal brine

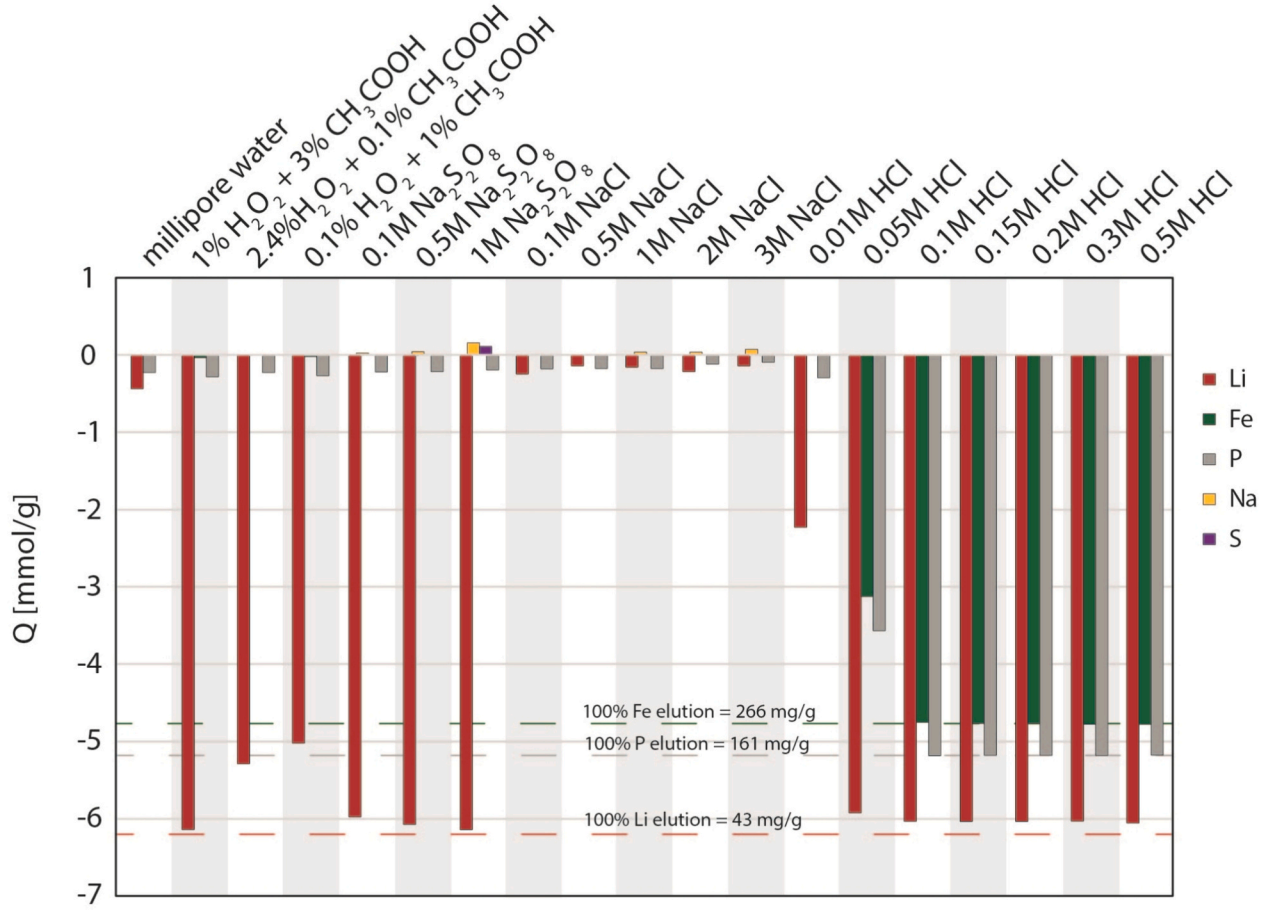

Fig. 5. Preliminary delithation experiments testing redox and ion exchange. Plot of different solutions vs. elution of Li, Fe and P and sorption of Na and S [mmol/g]. The experiments were conducted at 25 °C, 5 g/L $LiFePO_4$ and 45 min (24 h for HCl experiments).

(Fig. 12c; Table 3) and the maximum Li sorption capacity in isotherm experiments with synthetic Neustadt-Glewe geothermal brine (Fig. 12d; Table 3). At all investigated conditions, Li has an approximately 10 times higher affinity for $FePO_4$ than the other elements, with K_d values of 0.1–0.8 (Fig. 12, Table 3). In the Neustadt-Glewe experiments, Na and S concentrations in $FePO_4$ are much higher than Li (Fig. 11d). The K_d values of Li are, however, still higher than those of Na and S (Fig. 12d, Table 3). Although As and Pb are sorbed to $FePO_4$ occasionally, it was not possible to calculate K_d values for these elements because of lacking fluid data due to analytical difficulties with the $Na_2S_2O_3$ additive. Different selectivity orders are identified: (1) Li>Ba>As>Zn>Mn>Sr>S>Ca>Na>Mg>K (3 h, Bruchsal kinetics); (2) Li>Ba>Zn>Mn>B>S>Si>Sr>Ca>Na>Mg>K (2.5–5.0 g/L $FePO_4$/brine ratio, Bruchsal isotherm); (3) Li>Ba>Mn>Sr>S>Ca>Na>Mg>K>Zn (4 h, Neustadt-Glewe kinetics); and (4) Li>Zn>Ba>Mn>Sr>Ca>Na>S>Mg>K (2.0 g/L $FePO_4$/brine ratio, Neustadt-Glewe isotherm). Iron and P are disregarded for the selectivity sequence since K_d values would reflect the dissolution of $FePO_4$. Initial P concentration in the sample is below detection limit (Table 2) and Fe concentration is depleted compared to the original brine composition due to ferric oxyhydroxide precipitation under laboratory conditions. The different selectivity sequences are summarized qualitatively to Li>Ba>Mn>Sr>Ca>Na>Mg>K. The K_d values of Zn and S are variable. Sulfur likely has a similar selectivity as Ca and Na (Fig. 12a, c, d). Arsenic, B and Si are only extracted in the Bruchsal experiments, robust data on their selectivity is therefore not generated by our experiments.

The complete dataset for all experiments performed with (synthetic) geothermal brine (supplementary data) shows that Li has the highest affinity to $FePO_4$, i.e. higher K_d values than other elements, at reaction times between 15 min – 5 days and an $FePO_4$/brine ratio of 0.25–25 g/L (Bruchsal), or 60 min – 3 days and 0.4–16 g/L (Neustadt-Glewe). Although K_d values are highest for Li in these ranges, a higher purity of the re-lithiated $FePO_4$ is reached in Bruchsal using a $FePO_4$/brine ratio of 2.5–10 g/L. At lower and higher $FePO_4$/brine ratios, a higher total amount of Na is extracted (Fig. 11b).

4. Discussion

4.1. Mineralogical implications

The 3430 cm^{-1} band in the $LiFePO_4$ FT-IR-ATR spectrum represents OH^- vibrations and its presence indicates adsorbed water vapor [33]. The bands at 1138 cm^{-1} (ν_3), 1030 cm^{-1} (ν_3) and 927 cm^{-1} (ν_1) are assigned to antisymmetric P – O stretching vibrations of the PO_4^{3-} anion [18,34]. The bands at 633 cm^{-1} (ν_4), 574 cm^{-1} ($\nu_4 + \nu_2$) and 545 cm^{-1} ($\nu_4 + \nu_2$) are assigned to O – P – O stretching vibrations of the PO_4^{3-} anion [18,35]. The vibration at wavenumber 633 cm^{-1}, however, may also be assigned to FeO_6 [36]. The occurrence of the vibration at 1238 cm^{-1} has been previously discussed by Ait-Salah et al. [36] and is assumed to represent a unique stretching vibration of the PO_4^{3-} anion, only occurring in the $FePO_4$ phase. The minor shift of bands in the FT-IR-ATR spectrum of the re-lithiated $FePO_4$ compared to the initial $LiFePO_4$ material may indicate the formation of defects or distortion of the PO_4 units, e.g. the shift of the band at 927 cm^{-1} to 934 cm^{-1}. The formation of defects in the crystal lattice is of importance regarding the sorbent reuse in multiple cycles, potentially affecting the Li diffusivity in *b* direction, which may reduce the Li sorption capacity of $FePO_4$ after multiple sorption – desorption cycles.

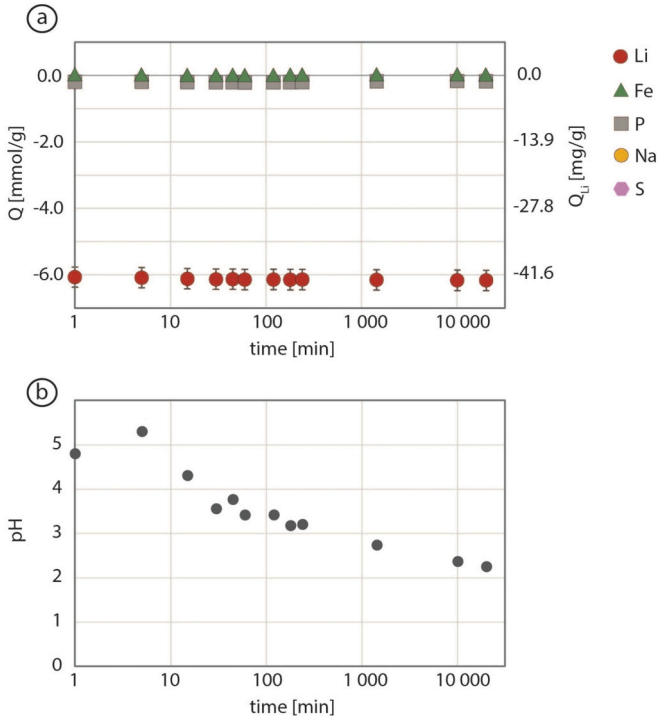

Fig. 6. Delithiation kinetics of $LiFePO_4$. a) Plot of sorption capacity [mmol/g] vs. reaction time [min] and b) pH value vs. reaction time [min]. The experiments were conducted at 25 °C, 0.1 M $Na_2S_2O_8$ and 5 g/L $LiFePO_4$.

The vibrations at low wavenumbers, i.e. at 496 cm^{-1} and 460 cm^{-1} are related to translational vibrations of Li^+ ions [18,35,36]. The bands that indicate the presence of Li^+ ions at 496 cm^{-1} and 460 cm^{-1}, disappear in the $FePO_4$ FT-IR-ATR spectrum (Fig. 4). Phase transition between $LiFePO_4$ and $FePO_4$ is complete since Li^+-ion characteristic bands are present or absent from the respective FT-IR-ATR spectra (Fig. 4).

The reversibility of delithiation – lithiation of LFP is also confirmed by the XRD data, because the pattern of re-lithiated $FePO_4$ is indistinguishable from orthorhombic triphylite from the initial $LiFePO_4$ (Fig. 2). The strong shift of some reflexes in the heterosite XRD pattern (Fig. 2II.), however, may indicate lattice distortion, possibly resulting from residual Li (Table 1) or the formation of crystal defects during phase transition. The occurrence of minor additional reflexes in the XRD patterns of re-lithiated samples (Fig. 2III., IV.) may indicate the formation of defects and/or mineral alteration. Thus, complete phase transition may induce structural defects that indicate aging of the material, which could be of significant importance for their application during numerous phase transition cycles. Mechanical cracking of LFP particles is interpreted as a result of stirring during the experiments (Fig. 1d, i, j). The mechanism of delithiation and lithiation of LFP is a reversible redox process and thus generally suitable for DLE.

The TG-DSC data indicate that $LiFePO_4$ and $FePO_4$ are stable under the specific DLE conditions between 60 and 80 °C (Fig. 3). The mass loss at temperatures <450 °C visible in both samples results from evaporation of adsorbed interparticle and crystal water from the nanocrystalline powder [1]. The presence of water is also evident from FT-IR-ATR spectra (Fig. 4). The two exothermic peaks at 573 °C and 654 °C (Fig. 3) reflect phase transitions in the $FePO_4$ lattice [1]. The increased mass loss at T >550 °C coincides with the exothermic peak indicating that this is linked to recrystallization potentially resulting from evaporation of more strongly bound crystal water [37]. The exothermic peak at 654 °C also coincides with a slight change in the mass loss, supporting further changes in the crystal lattice at these temperatures.

The mass of $LiFePO_4$ remains quite constant until ~420 °C,

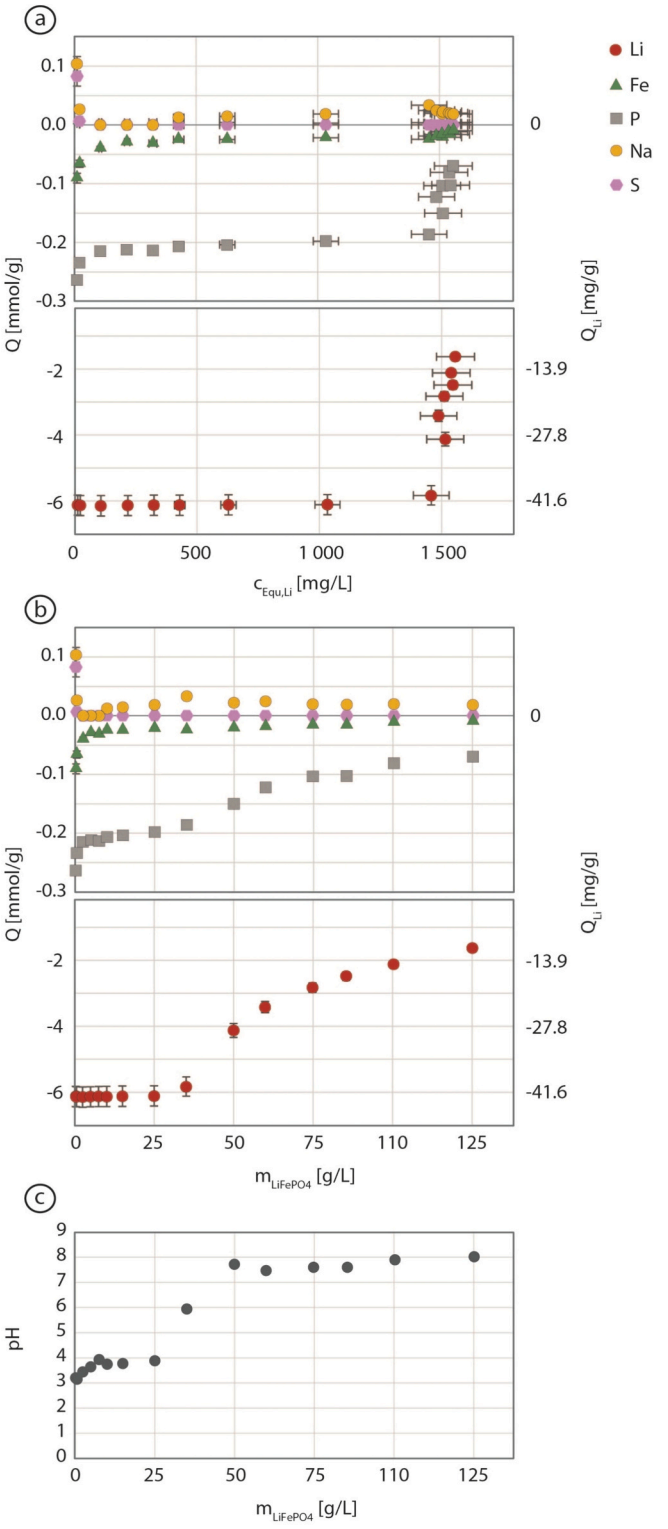

Fig. 7. Delithiation isotherm plot of a) sorption capacity [mmol/g] vs. equilibrium Li concentration [mg/L], b) $LiFePO_4$/fluid ratio [g/L] and c) pH value vs. $LiFePO_4$/fluid ratio [g/L]. The experiments were conducted at 25 °C, 0.1 M $Na_2S_2O_8$ and 60 min.

indicating that it contains less adsorbed interparticle water than $FePO_4$, which was produced by $LiFePO_4$ oxidation in aqueous solution. Mass loss between 420 and 550 °C contradicts the exothermic behaviour with a peak at 538 °C. The mass loss may result from water evaporation but endothermic peaks are lacking. The exothermic peak may be linked to

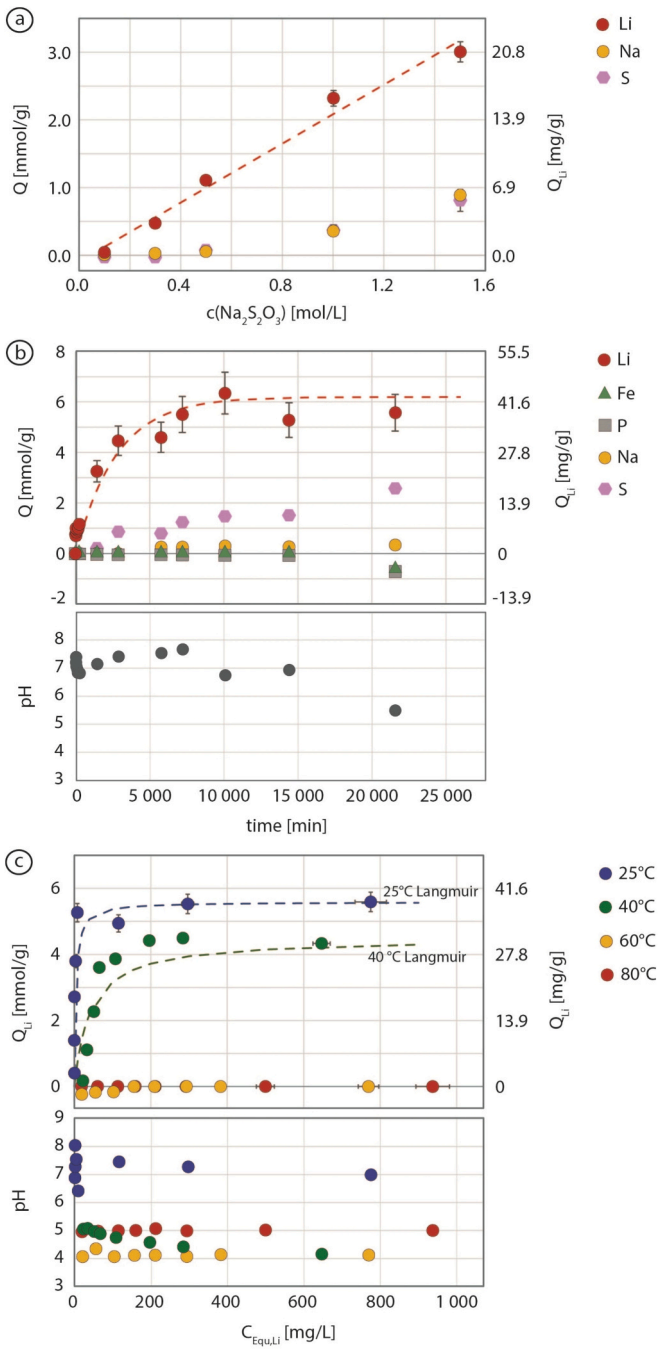

Fig. 8. Isotherms derived from experiments of synthetic LiCl + $Na_2S_2O_3$ solutions. a) Li, Na and S sorption capacity [mmol/g] vs. $Na_2S_2O_3$ concentration [mol/L]. The dashed line shows the linear relationship between lithiation and additive concentration. The experiments were conducted at 25 °C, 5 g/L $FePO_4$, 24 h and 200 mg/L initial Li concentration, b) lithiation kinetics in sorption capacity [mmol/g] vs. reaction time [min] and pH value vs. reaction time [min] at 25 °C, 5 g/L $FePO_4$/volume ratio and 200 mg/L initial Li concentration. The dashed line represents the PFO kinetic model and c) lithiation isotherm, plotted with sorption capacity [mmol/g and mg/g] vs. equilibrium Li concentration [mg/L] and pH value vs. equilibrium Li concentration [mg/L] at 25, 40, 60 and 80 °C. The experiments were conducted with 5 g/L $FePO_4$ for 7 days. The dashed lines illustrate the Langmuir models at 25 and 40 °C.

recrystallization processes, potentially caused by the loss of strongly bound crystal water [37]. This, however, is difficult to interpret and remains unclear without further analyses and detailed structural information. At higher temperatures, $LiFePO_4$ shows endothermic behaviour

Table 2
Chemical composition of the natural and synthetic geothermal brines from Bruchsal and Neustadt-Glewe before and after mixing with 0.5 M $Na_2S_2O_3$.

Analyte [mg/L]	Geothermal brine Bruchsal, Germany	Bruchsal brine + additive, before DLE	Geothermal brine Neustadt-Glewe, Germany	Synthetic Neustadt-Glewe brine + additive, before DLE
Li	155	158	11	11
Na	35,600	57,390	74,700	98,530
K	3240	3250	830	920
Mg	340	340	1340	1320
Ca	7440	7270	8300	8200
S	130	32,900	260	32,360
Rb	24	–	1.3	–
Cs	13	–	0.1	–
Sr	350	360	500	490
Ba	8.6	5.9	5.2	3.9
B	41	37	0.05	<0.009
SiO_2	90	45	32	<0.007
Pb	3.6	–	0.4	–
As	7.8	2.8	<0.0001	<0.002
Mn	24	21	12	7.9
Zn	14	7.1	3	2.1
Al	0.03	<0.07	<0.0002	<0.07
P	<0.0003	<0.003	<0.0003	<0.003
Sb	0.2	–	<0.000009	–
Ti	<0.0001	–	<0.0001	–
V	0.002	–	0.004	–
Cr	0.002	<0.003	0.004	<0.003
Fe	44	<0.0001	77	<0.0001
Co	0.005	<0.0003	<0.000009	<0.0003
Ni	0.005	<0.007	<0.00003	<0.007
Cu	0.02	<0.003	<0.00006	<0.003
Cd	0.08	<0.0002	0.005	<0.0002

up to 652 °C resulting from changed thermal conductivity properties of $LiFePO_4$ after previous water loss. This is followed by an exothermic behaviour with a two-step mass increase until 863 °C, potentially reflecting Fe oxidation and further recrystallization or N_2 sorption, followed by subsequent recrystallization. Melting of $LiFePO_4$ begins at 860 °C, whereas $FePO_4$ is more stable and starts melting at approximately 950 °C. After heating to 1000 °C and cooling to room temperature, the BSE images of the sample material confirm melt formation in both materials (Fig. 3b, c). Spinifex textures, also typically occurring in olivine-rich samples in the nature that indicate cooling under low nucleation rates and fast crystal growth rates [38] are visible in the $LiFePO_4$ sample (Fig. 3b). The phases that crystallized from the $FePO_4$ sample during heating to 1000 °C, are orthorhombic and triclinic (Fig. 3c). The orthorhombic crystals may represent euhedral heterosite, whereas the triclinic crystals may either represent kabalovite ($Fe_3^{+II}Fe_4^{+III}(PO_4)_6$) or nabateaite ($Fe_2P_2O_7$) [39,40].

4.2. Delithiation

Delithiation using NaCl does not elute Li significantly by ion exchange and $LiFePO_4$ is dissolved using HCl. Therefore, oxidation agents are regarded as most promising for $LiFePO_4$ delithiation. The oxidation agent $Na_2S_2O_8$ is proven to provide the highest delithiation capacity at the highest $LiFePO_4$ stability (Fig. 5).

The delithiation of $LiFePO_4$ is complete, reaching the maximum delithiation capacity of 42–43 mg/g (Fig. 7a, b), equal to the concentration of Li in $LiFePO_4$, supporting the crystallographic data (Figs. 2, 4). This indicates that the amount of anti-site defects in the initial $LiFePO_4$ sample is low [26].

Elution of P, Fe and Li is an effect occurring at low $LiFePO_4$/fluid ratios and pH <4 (Fig. 7b, c). No linear correlation is observed between elution and $LiFePO_4$/fluid ratio (Fig. 7b), and no increased Fe and P elution is observed during kinetic delithiation experiments at pH as low as 2.3 (Fig. 6b). Thus, both a $LiFePO_4$/fluid ratio <25 g/L and pH <4

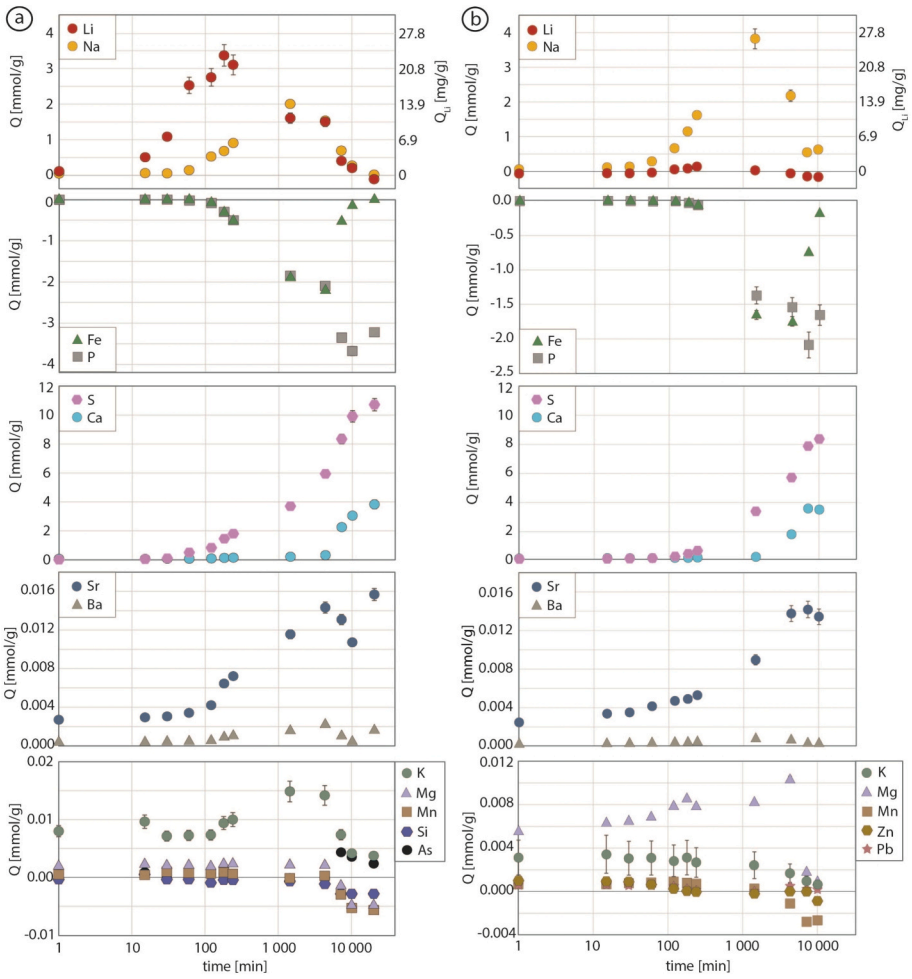

Fig. 9. Lithiation kinetics from geothermal brines plotted as sorption capacity [mmol/g] vs. reaction time [min]. The experiments were conducted at 60 °C, 5 g/L $FePO_4$, 160 mg/L and 10 mg/L initial Li concentration for a) Bruchsal and b) Neustadt-Glewe geothermal brines, respectively.

seem to affect $LiFePO_4$ stability negatively and should be avoided in DLE.

4.3. Lithiation experiments with pure LiCl – $Na_2S_2O_3$ solution

$FePO_4$ lithiation is a redox reaction of $Fe^{+III} \rightarrow Fe^{+II}$ under consumption of $Na_2S_2O_3$ (F.4) [24].

$$2\,Li^{+} + 2\,Fe^{+III}PO_4 + 2\,\left[S_2^{+II}O_3\right]^{2-} \rightarrow 2\,LiFe^{+II}PO_4 + \left[S_2^{0}\left(S^{+V}O_3\right)_2\right]^{2-} \quad \text{(F.4)}$$

Li sorption increases within 24 h with increasing $Na_2S_2O_3$ concentration (Fig. 8a). Thus, the mechanism of lithiation shows positive correlation of sorption kinetics and sorption capacity with increasing reducing agent concentration.

$FePO_4$ is not affected by the $Na_2S_2O_3$ additive since Fe and P loss is below the detection limit during 24 h reaction time at 25 °C. The increasing sorption of Na and S with increasing $Na_2S_2O_3$ concentration may indicate insufficient rinsing of the $FePO_4$ after filtration, rather than sorption to $FePO_4$ (Fig. 8a). However, in kinetic experiments using 0.5 M $Na_2S_2O_3$, Na and S are progressively sorbed to $FePO_4$ with longer reaction time (Fig. 8b). The observation cannot be explained by rinsing effects since the initial concentration of $Na_2S_2O_3$ and the $FePO_4$/fluid ratio are constant. In a DLE process, lithiation should thus be stopped immediately after reaching equilibrium, reducing the sorbed amount of Na and S and avoiding $FePO_4$ dissolution (Fig. 8b).

The rather long equilibration time of seven days (Fig. 8b) results from the low, 0.5 M additive concentration and will be faster if a higher concentration of $Na_2S_2O_3$ is used (Fig. 8a). The lithiation kinetics fit well with a pseudo-first-order (PFO) kinetic model (F.5), with the variables $k_1 = 0.00036248\ min^{-1}$ (rate constant in the PFO equation), $Q_{Equ} = 43$ mg/g (maximum Li uptake) and Q_t (Li uptake at any time t) [31].

$$Q_t = Q_{Equ}\left(1 - e^{-k_1 t}\right). \quad \text{(F.5)}$$

The Li sorption at 25 and 40 °C (Fig. 8c) is described by a Langmuir isotherm with the K_L values 0.2445 (25 °C) and 0.0239 (40 °C) derived from the Scratchard linearization of the Langmuir model [31]. The steep initial slope of the isotherm at 25 °C indicates a high affinity of $FePO_4$ to Li [31], which is for a prerequisite of DLE. Temperatures >40 °C have a negative influence on the process (Fig. 8c). The sorption of Li to $FePO_4$ is thus different from many other sorption processes, where kinetics are slowest at low temperatures due to slower ion diffusion rates and equilibrium is identified by a stable plateau with longer reaction time [e.g., 41,42]. At 25 °C, the initial pH is 9.0–9.1, whereas the initial pH of the solution at 40 °C is 8.5–9.0, at 60 °C pH = 5.0–5.3 and at 80 °C pH = 5.0–5.5. The pH ≤5.5 at 60 and 80 °C may be the reason for Li not intercalating into $FePO_4$ at these temperatures. After the experiments, the pH is 6.4–8.0 (25 °C), 4.2–5.1 (40 °C), 4.1–4.4 (60 °C) and 5.0 (80 °C), respectively (Fig. 8c). The acidification during the experiments, however, does not correlate with the (equilibrium) Li concentration and is thus not a result of a potential additional $Li^+ - H^+$ ion exchange process. It seems more likely that the $Na_2S_2O_3$ additive becomes unstable during Li extraction and/or at elevated temperatures, leading to acidification during heating already prior to the start of the experiments.

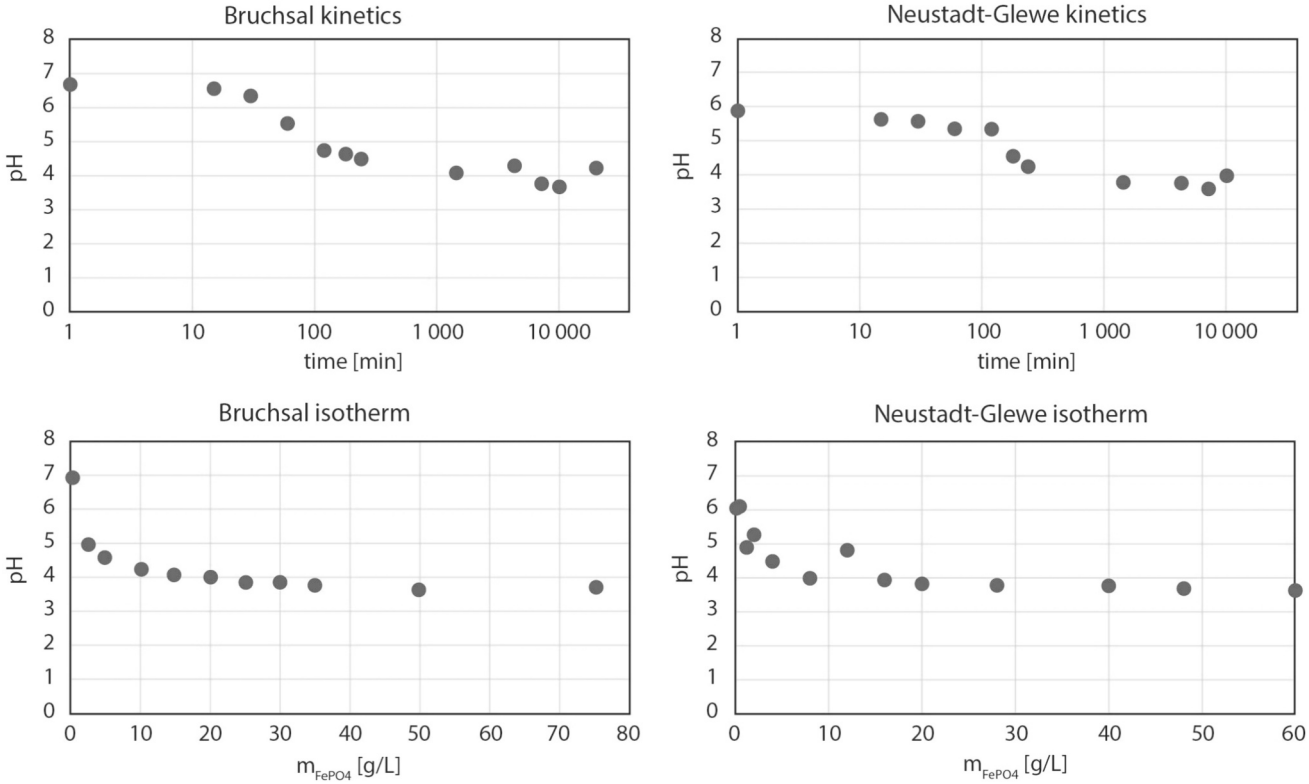

Fig. 10. pH variations in DLE experiments with geothermal brines. The experiments were conducted at 60 °C and initial Li concentrations of 160 mg/L (Bruchsal) and 10 mg/L (Neustadt-Glewe). A $FePO_4$/brine ratio of 5 g/L was used in kinetic experiments and the stirring time in isotherm experiments was 3 h (Bruchsal) and 4 h (Neustadt-Glewe).

4.4. *Lithiation from geothermal brines*

The Li sorption kinetics in experiments using both brines does not reach a plateau (Fig. 9), known from sorption kinetics in general [e.g., 41,42]. Lithium and Na show the same sorption behaviour, indicating that they are both intercalated into $FePO_4$, sharing the same sorption site in M1. The time gap between Li and Na sorption may be a result of different diffusivity. Possibly the Li diffusivity in *b* direction during phase transformation of $FePO_4$ to $LiFePO_4$, progressively expands the unit cell up to 6.8 vol% [2] and thereby opens the pathway for Na to intercalate into LFP in *b* direction.

The Bruchsal lithiation isotherm is described by a Langmuir sorption behaviour for equilibrium Li concentrations of <80 mg/L (Fig. 11a). In the isotherm experiments, Na shows a contradictory behaviour to Li (Fig. 11b), confirming that Na and Li are competing ions in the M1 sorption site. After the maximum Li sorption in kinetic experiments, $FePO_4$ dissolution starts and Li is eluted into the brine (Fig. 9). Iron and P dissolution starts after 1–2 h reaction time, i.e. shortly after Na starts to intercalate into $FePO_4$ (Fig. 9), and is at maximum when Na sorption is at maximum. Similar to the kinetic experiments, the $FePO_4$ dissolution positively correlates with the Na sorption and decreases at $FePO_4$/brine ratios >5 g/L, (Fig. 11b). Since the intercalation of Na into $FePO_4$ leads to an expansion of the unit cell volume by 16.6 vol% [14], the stability of $FePO_4$ may be negatively influenced by Na intercalation, leading to its dissolution.

The observed surface roughness of the LFP particles is the result of daughter crystals that nucleate on their surface. EDX and XRD data indicate that native sulfur may occur on the surface of the LFP, whereas the euhedral crystals are identified as gypsum (Fig. 2V.). The samples from experiments with synthetic geothermal brine of Neustadt-Glewe composition show the same: No secondary phases are visible until the maximum sorption capacity is reached (Fig. 1g). At longer reaction time, however, native sulfur and gypsum precipitate like in the other samples (Fig. 1f, h). In the experiments with synthetic brine, native sulfur does not occur on the LFP surface but forms larger aggregates (Fig. 1f, h). The precipitation of gypsum and native sulfur explains the S and Ca geochemical data (Fig. 9) and confirms that S and Ca are not mainly sorbed to $FePO_4$, but precipitated in other phases.

The extracted amount of Ba and Sr is similar for both tested brine compositions, which is explained by similar starting concentrations (Table 2). Due to the similar geochemical behaviour of Sr, Ba and Ca, the increase in Sr and Ba extraction may be an effect of progressing gypsum precipitation, rather than sorption to $FePO_4$. Gypsum and native sulfur are known to precipitate due to decreasing pH [43–45]. The extraction of Ca, S, Ba and Sr, i.e. gypsum and sulfur precipitation, already occurs before the dissolution of $FePO_4$ starts (Fig. 9); and the dissolution of Fe and P starts before the equilibrium pH at ~5.5 is reached. This indicates limited $FePO_4$ stability at pH <5.5 (Fig. 10). The decrease in pH is a function of the $FePO_4$/brine ratio (Fig. 10) and the sorbent stability behaves differently compared to delithiation experiments, due to the different matrices, i.e. $Na_2S_2O_8$ for delithiation and $Na_2S_2O_3$ for lithiation.

It is likely that the decrease in pH leading to $FePO_4$ dissolution and co-precipitation of secondary phases is a result of $Na_2S_2O_3$ instability. Disproportionation of $Na_2S_2O_3$ (F.6) [45] leads to SO_4^{2-} formation and H_2S degassing, recognized by the characteristic smell in the laboratory during pre-heating and during the experiments. Since the reaction vessels are closed during the experiments, a liquid/vapor equilibrium may form, leading to brine acidification (F.7) [45]. Disproportionation may be the reason that no Li was extracted from LiCl solutions at 60–80 °C since degassing of H_2S may be catalyzed by increasing temperature. Thus, $Na_2S_2O_3$ may already be fully consumed during the seven days reaction time at high temperatures or during pre-heating of the partially closed vessels (to prevent overpressure), not being able to support the redox reaction. The SO_4^{2-} species forms gypsum in reaction with Ca^{2+} ions from the geothermal brine. Thus, gypsum precipitation is not

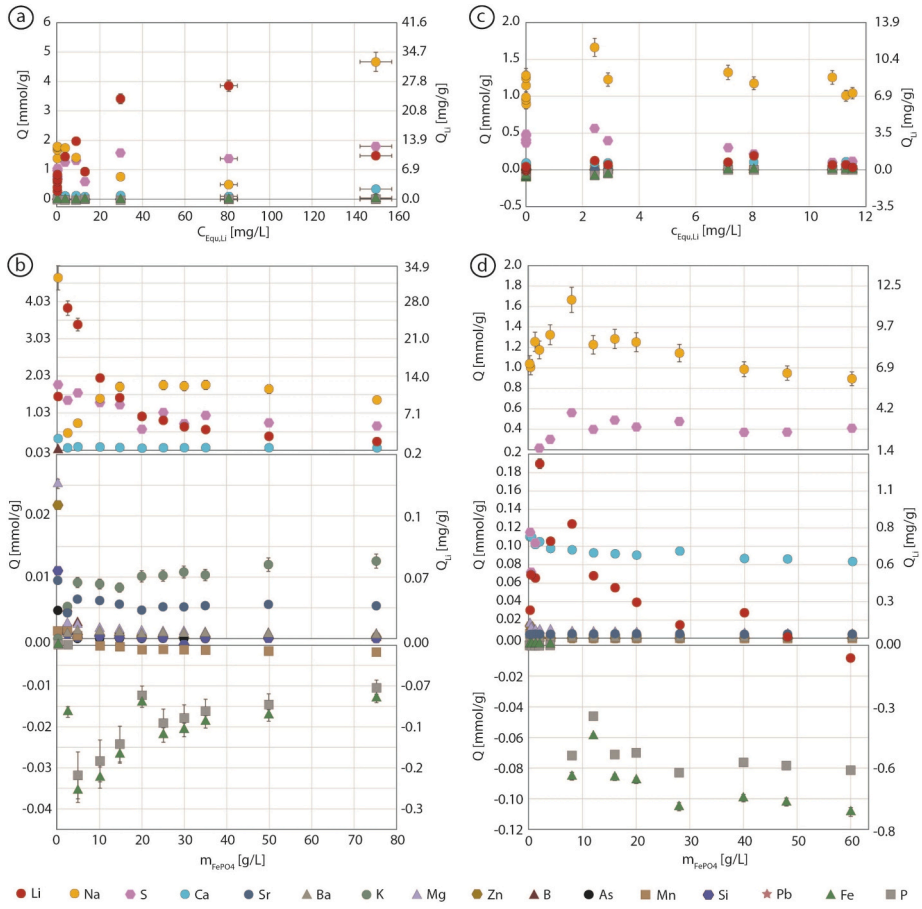

Fig. 11. Lithiation isotherms from geothermal brines. a) Sorption capacity (Q) in mmol/g vs. equilibrium Li concentration ($C_{Equ,Li}$) in mg/L (Bruchsal), b) sorption capacity (Q) in mmol/g vs. $FePO_4$/brine ratio [g/L] (Bruchsal), c) sorption capacity (Q) in mmol/g vs. equilibrium Li concentration ($C_{Equ,Li}$) in mg/L (Neustadt-Glewe) and d) sorption capacity (Q) in mmol/g vs. $FePO_4$/brine ratio [g/L] (Neustadt-Glewe). The experiments were conducted at 60 °C, 160 mg/L and 10 mg/L initial Li concentration for a + b) Bruchsal and c + d) Neustadt-Glewe geothermal brines, respectively. The reaction time was 3 h with Bruchsal and 4 h with Neustadt-Glewe geothermal brine.

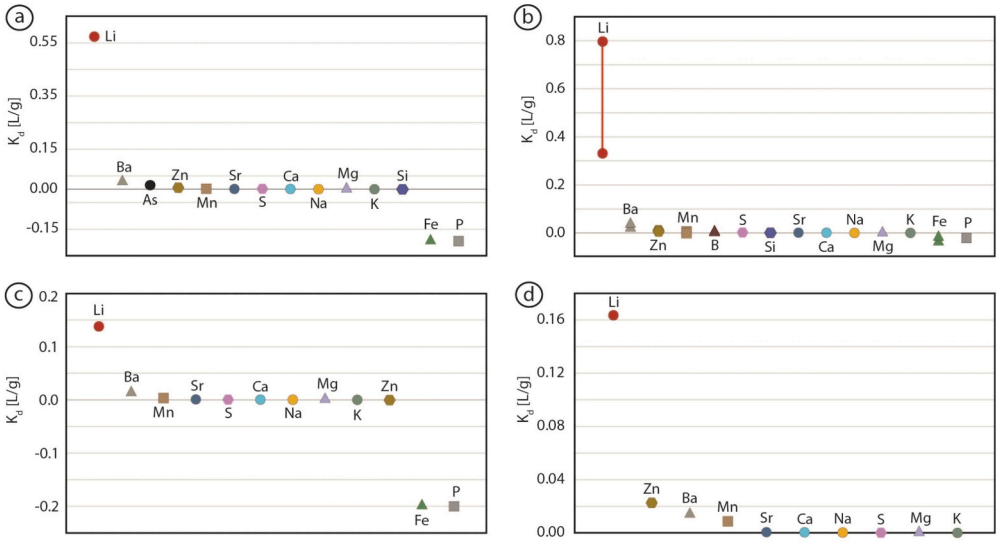

Fig. 12. Distribution coefficients for optimal Li extraction conditions. The experiments were conducted at 60 °C and initial Li concentrations of 160 mg/L (Bruchsal) and 10 mg/L (Neustadt-Glewe). a) Three hours reaction time (Bruchsal), b) 2.5–5 g/L $FePO_4$/brine ratio in isotherm experiments (Bruchsal), c) four hours reaction time (Neustadt-Glewe) and d) 2 g/L $FePO_4$/brine ratio in isotherm experiments (Neustadt-Glewe).

Table 3
Equilibrium Li concentration, sorption capacity [mg/g and mmol/g], K_d value and selectivity estimation for different elements at maximum Li intercalation in kinetics and isotherm experiments with geothermal brines.

	Li	Na	K	Mg	Ca	Sr	Ba	B	Si	Pb	P	As	S	Mn	Fe	Zn
Bruchsal kinetics, 3 h																
C_{Equ} [mg/L]	41	58,640	3240	330	7390	360	4.7	36	22	–	47	3.0	32,530	21	90	9.3
Load [mg/g]	23	16	0.4	0.06	5.4	0.6	0.1	<002	−0.01	<LOQ	−9.2	0.05	47	0.05	−17	0.06
Load [mmol/g]	3.37	0.68	0.01	0.002	0.13	0.01	0.001	<0.0002	−0.0004	<LOQ	−0.3	0.001	1.46	0.001	−0.31	0.001
K_d value [L/g]	0.5729	0.0003	0.0001	0.0001	0.0007	0.0016	0.0267	–	−0.0005	–	−0.1947	0.0157	0.0014	0.0023	−0.1947	0.0059
Selectivity order	1	9	11	10	8	6	2	–	12	–	14	3	7	5	13	4
Bruchsal isotherm, 2.5–5 g/L LFP/brine ratio																
C_{Equ} [mg/L]	30–81	54,890–55,020	3100	330	6910–6940	350	5.3–5.8	37	19–20	–	<LOQ – 48	<LOQ	32,910–33,130	19	23–97	6.0–6.1
Load [mg/g]	24–27	11–17	0.2–0.4	0.06	3.8–5.0	0.4–0.6	0.1–0.2	0.03–0.05	0.01–0.02	<LOQ	<LOQ – −1	<LOQ – 0.1	44–50	0.03–0.08	−1 to −2	0.04–0.06
Load [mmol/g]	3.41–3.85	0.49–0.76	0.01	0.02	0.09–0.12	0.004–0.01	0.001	0.003–0.005	0.000–0.001	<LOQ	<LOQ – −0.03	<LOQ – 0.001	1.37–1.57	0.0005–0.001	−0.02 to −0.04	0.001
K_d value [L/g]	0.3313–0.7965	0.0002–0.0003	0.0001	0.0001	0.0005–0.0007	0.001–0.0016	0.0183–0.0314	0.0007–0.0015	0.0003–0.0011	–	−0.0204	–	0.0013–0.0015	0.0013–0.0042	−0.0204 to −0.0393	0.0067–0.0097
Selectivity order	1	10	12	11	9	8	2	5	7	–	14	–	6	4	13	3
Neustadt-Glewe kinetics, 4 h																
C_{Equ} [mg/L]	6.9	99,630	890	1300	8330	510	4.7	–	–	–	9.7	–	32,810	12	18	2.7
Load [mg/g]	1.0	37	0.1	0.2	4.1	0.5	0.1	–	–	0.02	−1.9	–	19	0.04	−3.7	−0.0003
Load [mmol/g]	0.14	1.62	0.003	0.01	0.10	0.01	0.0004	–	–	0.0001	−0.06	–	0.58	0.001	−0.07	−0.0000
K_d value [L/g]	0.1381	0.0004	0.0001	0.0001	0.0005	0.0009	0.01246	–	–	–	−0.2	–	0.0006	0.0033	−0.2	−0.0001
Selectivity order	1	7	9	8	6	4	2	–	–	–	12	–	5	3	11	10
Neustadt-Glewe isotherm, 2 g/L LFP/brine ratio																
C_{Equ} [mg/L]	8.1	97,970	950	1330	8050	460	2.9	–	–	–	<LOD	–	32,440	11	<LOQ	2.5
load [mg/g]	1.3	27	0.1	0.2	4.2	0.4	0.04	–	–	0.2	<LOD	–	6.9	0.1	<LOQ	0.1
load [mmol/g]	0.19	1.18	0.003	0.01	0.1	0.005	0.0003	–	–	0.001	<LOD	–	0.22	0.002	<LOQ	0.001
K_d value [L/g]	0.1636	0.0003	0.0001	0.0002	0.0005	0.0009	0.0138	–	–	–	–	–	0.0002	0.0087	–	0.0227
selectivity order	1	7	10	9	6	5	3	–	–	–	–	–	8	4	–	2

observed in the experiments with LiCl + $Na_2S_2O_3$ solution. According to (F.8), H_2S can react with SO_4^{2-} and H^+ to precipitate native sulfur [44]. An additional reaction that may take place is the decomposition of $Na_2S_2O_3$ with protons (e.g., from H_2S equilibrium in the closed vessels) that causes native sulfur precipitation (F.9) [45]. The combination of all the described reactions explains the processes observed in our experiments.

$$[S_2O_3]^{2-} + H_2O \rightleftarrows H_2S\uparrow + SO_4^{2-} \quad \text{(F.6)}$$

$$H_2S \rightleftarrows H^+ + HS^- \rightleftarrows 2H^+ + S^{2-} \quad \text{(F.7)}$$

$$3H_2S + SO_4^{2-} + 2H^+ \rightarrow 4S^0\downarrow + 4H_2O \quad \text{(F.8)}$$

$$Na_2S_2O_3 \xrightarrow{+2HCl,\,-2NaCl} H_2S_2O_3 \xrightarrow{-H_2SO_3} \frac{1}{n}S_n \quad \text{(F.9)}$$

No secondary phases, like gypsum or native sulfur are, however, observed in the isotherm experiments. The dissolution of Fe and P is significantly lower than in kinetic experiments which may result from higher $FePO_4$ stability due to minor Na intercalation and lattice expansion at shorter reaction times. In addition, the solution acidifies with increasing $FePO_4$/brine ratio to the same degree as in kinetic experiments (Fig. 10). Native sulfur and gypsum precipitation are thus not solely controlled by pH decrease but also by kinetics.

The strong decrease in Fe elution in kinetic experiments after the maximum (Fig. 9) may be explained by the formation of a new phase, which is, however, not detected by XRD or visible in SEM. It is more likely that Fe is a trace compound in the gypsum precipitate [46], since P elution remains at maximum at long stirring times.

A pH adjustment during lithiation of $FePO_4$ is not necessary since maximum Li intercalation is achieved at short reaction times, where Fe and P elution is low and the extraction process should be immediately stopped due to decreasing Li selectivity at longer reaction times, as discussed previously (Fig. 9). To improve stability of $FePO_4$ at reaction times >24 h, however, buffering may be advantageous due to $Na_2S_2O_3$ decomposition and brine acidification.

Since Na and S are already compounds in the geothermal brine, the increase in Na and S concentration in the geothermal brine by using $Na_2S_2O_3$ as reducing agent is regarded as uncritical. To overcome the challenge regarding limited $Na_2S_2O_3$ stability, another reducing agent may be used instead, e.g. ascorbate, iodide or hydride compounds, like NaI, $(AlH_3)_x$ or $NaBH_4$ [14,25,27,47]. The use of an ascorbate reducing agent, however, might be challenging for the DLE application in geothermal brines since ascorbic acid degrades with increasing fluid temperature [48]. Oxidation of ascorbate forms dehydroascorbate, which further degrades into different products, e.g. furan-2-carboxylic acid or furan-2-carbaldehyde [49,50]. Both are hazardous to water and the latter is potentially carcinogenic, which is disadvantageous for DLE from geothermal brines [51,52]. Iodine concentration in the geothermal brines is usually below detection limit and the introduction of iodine into the brine might be critical with respect environmental and legal aspects [53,54]. Aluminium hydride is thermally stable to up to 160 °C [55]. However, it is sensitive to moisture, i.e. it reacts strongly with water forming $Al(OH)_3$ and H_2 [45,55]. Sodium and B are components of geothermal brines, rendering $NaBH_4$ a potential option. Furthermore, hydrogen gas may be applied as reducing agent. Therefore, experiments to test the applicability of hydrides or hydrogen are suggested to substitute $Na_2S_2O_3$.

The kinetics of different elements, like Li and Na, Fe and P or Ca, S, Ba and Sr, is similar in extraction experiments from brines that have significantly different initial Li concentrations, i.e. Bruchsal and Neustadt-Glewe (Table 2). This emphasizes the reproducibility of the results and similar underlying extraction mechanisms. In electrochemical Li extraction, the selectivity is controlled by adjustment of the applied voltage [20,22]. The selectivity of the chemical DLE process using $FePO_4$ may be controlled by adjusting the reaction time, instead. The steep initial slope of the isotherms derived from experiments using LiCl + $Na_2S_2O_3$ solutions (Fig. 8c) and the successful extraction of Li from saline geothermal brine (Section 3.5) confirm high Li selectivity of $FePO_4$. The DLE process, however, should be adjusted to optimal conditions to successfully extract Li among other elements, i.e. 3–4 h reaction time and an $FePO_4$/brine ratio of 2–10 g/L is determined in our experiments. Minor Fe and P loss, the potential formation of defects in the crystal lattice and variations in the maximum Li sorption capacity of LFP depend on the experimental setup and geochemical brine composition. This might affect the recycling potential of the sorbent and is of significance for the LFP reuse in multiple DLE cycles. Since the results for both brine compositions are similar, the data and identified optimal conditions are likely also applicable to other (unbuffered) brines, but should, however, be tested and verified.

The lithiation isotherms for the Bruchsal and Neustadt-Glewe geothermal brines show that the Li extraction using $FePO_4$ is successful for brines with initial Li concentrations between 10 and 160 mg/L (Table 2), reaching a Li recovery of >99 % within one extraction cycle (Fig. 11a, c). This is an advantage for a chemical DLE process using LFP compared to electrochemical DLE using LFP. Comparably high Li recoveries of 98 % can be reached by electrochemical techniques, but several delithiation – lithiation cycles are needed, e.g. 3 cycles from a LiCl solution containing 60 mg/L Li [22]. Eight extraction cycles are needed to recover 91 % Li from a low saline brine [21]. Thus, more cycles may be required to reach as high Li recoveries from high saline geothermal brines, but experimental data is sparse [20,22].

5. Conclusions

Lithium completely de-intercalates from and re-intercalates into $LiFePO_4$ (LFP) in a mineralogically and chemically fully reversible redox process. This study investigates the application of LFP for the direct Li extraction (DLE) from two chemically different geothermal brines in Germany. The Li-poor phase, used for DLE, is orthorhombic heterosite $FePO_4$. The Li-rich phase is orthorhombic triphylite $LiFePO_4$.

A starting LFP cathode material is delithiated using 0.1 M $Na_2S_2O_8$. Within 1 min reaction time, 43 mg/g Li are successfully extracted at an $LiFePO_4$/volume ratio of 0.5–35 g/L. Lithiation of $FePO_4$ is positively correlating with the concentration of the reducing agent ($Na_2S_2O_3$). For optimal Li extraction in a 0.5 M $Na_2S_2O_3$ matrix, a reaction time of 3–4 h and an $FePO_4$/brine ratio of 2–10 g/L is estimated. The Li extraction process should immediately be stopped when the highest Li sorption capacity is achieved. Otherwise, Li extraction is inefficient, $FePO_4$ stability decreases and secondary phases, like gypsum and native sulfur, precipitate. >99 % Li are recovered from the Bruchsal geothermal brine and the synthetic brine of Neustadt-Glewe in the laboratory, confirming a similar elemental behaviour and the reproducibility of the results for different brines.

We show that LFP is successfully used for Li extraction from geothermal brine in Germany in a purely chemical DLE process with very high recovery and high Li-load within one cycle. Limitations are few crystal defects that are imposed during the process, which indicates potential sorbent aging, and the $Na_2S_2O_3$ redox agent that causes side reactions and that better would be replaced by an alternative material during up-scaling. A major challenge for upscaling the presented technique to industrial scale is the handling of nanoparticles in a high flow regime like geothermal power plants. Technical solutions or formulation approaches and the investigation of the Li sorption performance of novel LFP-based materials are thus required.

CRediT authorship contribution statement

Rebekka Reich: Conceptualization, Methodology, *V*alidation, Formal analysis, Investigation, Resources, Writing - Original Draft, Writing - Review & Editing, Visualization, Project administration. **Elisabeth Eiche:** Conceptualization, Methodology, Resources, Writing -

Original Draft, Writing - Review & Editing, Supervision, Project administration, Funding acquisition. **Jochen Kolb:** Conceptualization, Methodology, Resources, Writing - Original Draft, Writing - Review & Editing, Supervision, Project administration, Funding acquisition.

Declaration of competing interest

The authors declare that they have no known competing financial interests or personal relationships that could have appeared to influence the work reported in this paper.

Data availability

Data will be made available on request.

Acknowledgements

We thank IBU-tec AG, Weimar, Germany for providing the LFP cathode material. We thank Julia Podszuweit and Günter Beuchle for the BET analysis. Laura Spitzmüller is acknowledged for performing FT-IR-ATR analyses. We thank Andrea Seibt for the experiments with synthetic Neustadt-Glewe geothermal brine. Nadine Hüll and Janine Wagner are acknowledged for sample digestion. Chantal Kotschenreuther and Maya Denker are acknowledged for their assistance with the ICP-OES and ICP-MS analyses, respectively. We thank Janine Wagner for her help during XRD data acquisition. Michèle Jungmann and the UnLimited project team members are thanked for their helpful contributions during all stages of this study. This research is part of the "UnLimited" project, funded by the German Federal Ministry for Economic Affairs and Climate Action under Grant O3EE4023D.

Appendix A. Supplementary data

Supplementary data to this article can be found online at https://doi.org/10.1016/j.desal.2024.117883.

References

[1] S.M. Zhang, J.X. Zhang, S.J. Xu, X.J. Yuan, T. Tian, Synthesis of nano-sized FePO4 cathode material via a microemulsion technique, Appl. Mech. Mater. 320 (2013) 675–682, https://doi.org/10.4028/www.scientific.net/AMM.320.675.
[2] A. Banday, R. Shahid, S.S. Meena, S. Yusuf, S. Murugavel, Effect of crystallite size on the phase transition behavior of heterosite FePO 4, Phys. Chem. Chem. Phys. 22 (2020) 15478–15487, https://doi.org/10.1039/D0CP02387F.
[3] J. Lee, P. Kumar, J. Lee, B.M. Moudgil, R.K. Singh, ZnO incorporated LiFePO4 for high rate electrochemical performance in lithium ion rechargeable batteries, J. Alloys Compd. 550 (2013) 536–544, https://doi.org/10.1016/j.jallcom.2012.10.092.
[4] A. Mauger, A. Ait-Salah, M. Massot, F. Gendron, K. Zaghib, C. Julien, Characterization of LiFePO4 at a Nanoscopic scale in relation to the mode of preparation, ECS Trans. 3 (2007) 57, https://doi.org/10.1149/1.2795106.
[5] C. Zhu, K. Weichert, J. Maier, Electronic conductivity and defect chemistry of heterosite FePO4, Adv. Funct. Mater. 21 (2011) 1917–1921, https://doi.org/10.1002/adfm.201002059.
[6] T. Maxisch, G. Ceder, Elastic properties of olivine Li x FePO 4 from first principles, Phys. Rev. B 73 (2006) 174112, https://doi.org/10.1103/PhysRevB.73.174112.
[7] G. Rousse, J. Rodriguez-Carvajal, S. Patoux, C. Masquelier, Magnetic structures of the triphylite LiFePO4 and of its delithiated form FePO4, Chem. Mater. 15 (2003) 4082–4090, https://doi.org/10.1021/cm0300462.
[8] A. Losey, J. Rakovan, J.M. Hughes, C.A. Francis, M.D. Dyar, Structural variation in the lithiophilite–triphylite series and other olivine-group structures, Can. Mineral. 42 (2004) 1105–1115, https://doi.org/10.2113/gscanmin.42.4.1105.
[9] J.L. Dodd, B. Fultz, R. Yazami, Determining the phase diagram of LixFePO4, ECS Transactions 1 (2006) 27, https://doi.org/10.1149/1.2209354.
[10] M. Wagemaker, D.P. Singh, W.J. Borghols, U. Lafont, L. Haverkate, V.K. Peterson, F.M. Mulder, Dynamic solubility limits in nanosized olivine LiFePO4, J. Am. Chem. Soc. 133 (2011) 10222–10228, https://doi.org/10.1021/ja2026213.
[11] N. Meethong, H.-Y.S. Huang, W.C. Carter, Y.-M. Chiang, Size-dependent lithium miscibility gap in nanoscale Li1− x FePO4, Electrochem. Solid St. 10 (2007) A134, https://doi.org/10.1149/1.2710960.
[12] F. Omenya, N.A. Chernova, Q. Wang, R. Zhang, M.S. Whittingham, The structural and electrochemical impact of Li and Fe site substitution in LiFePO4, Chem. Mater. 25 (2013) 2691–2699, https://doi.org/10.1021/cm401293r.
[13] A. Moretti, G. Giuli, F. Nobili, A. Trapananti, G. Aquilanti, R. Tossici, R. Marassi, Structural and electrochemical characterization of vanadium-doped LiFePO4 cathodes for lithium-ion batteries, J. Electrochem. Soc. 160 (2013) A940, https://doi.org/10.1149/2.133306jes.
[14] J. Lu, S.C. Chung, S.-i. Nishimura, A. Yamada, Phase diagram of olivine Na x FePO4 (0< x< 1), Chem. Mater., 25 (2013) 4557–4565, doi:https://doi.org/10.1021/cm402617b.
[15] A.S. Andersson, B. Kalska, L. Häggström, J.O. Thomas, Lithium extraction/insertion in LiFePO4: an X-ray diffraction and Mössbauer spectroscopy study, Solid State Ion. 130 (2000) 41–52, https://doi.org/10.1016/S0167-2738(00)00311-8.
[16] M. Gadgil, S. Kulshreshtha, Study of FePO4 catalyst, J. Solid State Chem. 111 (1994) 357–364, https://doi.org/10.1006/jssc.1994.1239.
[17] G. Kobayashi, S.i. Nishimura, M.S. Park, R. Kanno, M. Yashima, T. Ida, A. Yamada, Isolation of solid solution phases in size-controlled LixFePO4 at room temperature, Adv. Funct. Mater. 19 (2009) 395–403, https://doi.org/10.1002/adfm.200801522.
[18] Y. Kuk, J. Hwang, D. Nam, J. Kim, Facile synthesis of high-performance LiFePO4-reduced graphene oxide composites using ball milling, Ionics 26 (2020) 2803–2812, https://doi.org/10.1007/s11581-019-03395-6.
[19] F. Larouche, F. Voisard, K. Amouzegar, G. Houlachi, P. Bouchard, A. Vijh, G. P. Demopoulos, Kinetics, mechanism, and optimization modeling of a green LFP Delithiation process developed for direct recycling of Lithium-ion batteries, Ind. Eng. Chem. Res. 62 (2023) 903–915, https://doi.org/10.1021/acs.iecr.2c03552.
[20] X. Liu, X. Chen, Z. Zhao, X. Liang, Effect of Na+ on Li extraction from brine using LiFePO4/FePO4 electrodes, Hydrometallurgy 146 (2014) 24–28, https://doi.org/10.1016/j.hydromet.2014.03.010.
[21] S. Sun, X. Yu, M. Li, J. Duo, Y. Guo, T. Deng, Green recovery of lithium from geothermal water based on a novel lithium iron phosphate electrochemical technique, J. Clean. Prod. 247 (2020) 119178, https://doi.org/10.1016/j.jclepro.2019.119178.
[22] Z. Zhao, X. Si, X. Liu, L. He, X. Liang, Li extraction from high mg/Li ratio brine with LiFePO4/FePO4 as electrode materials, Hydrometallurgy 133 (2013) 75–83, https://doi.org/10.1016/j.hydromet.2012.11.013.
[23] K. Liu, Q. Tan, L. Liu, J. Li, Acid-free and selective extraction of lithium from spent lithium iron phosphate batteries via a mechanochemically induced isomorphic substitution, Environ. Sci. Technol. 53 (2019) 9781–9788, https://doi.org/10.1021/acs.est.9b01919.
[24] N. Intaranont, N. Garcia-Araez, A. Hector, J. Milton, J. Owen, Selective lithium extraction from brines by chemical reaction with battery materials, J. Mater. Chem. A 2 (2014) 6374–6377, https://doi.org/10.1039/C4TA01101E.
[25] C. Kuss, M. Carmant-Dérival, N.D. Trinh, G. Liang, S.B. Schougaard, Kinetics of Heterosite Iron phosphate Lithiation by chemical reduction, J. Phys. Chem. C 118 (2014) 19524–19528, https://doi.org/10.1021/jp502346f.
[26] D. Lepage, F. Sobh, C. Kuss, G. Liang, S. Schougaard, Delithiation kinetics study of carbon coated and carbon free LiFePO4, J. Power Sources 256 (2014) 61–65, https://doi.org/10.1016/j.jpowsour.2013.12.054.
[27] J. Xiong, Z. Zhao, D. Liu, L. He, Direct lithium extraction from raw brine by chemical redox method with LiFePO4/FePO4 materials, Sep. Purif. Technol. 290 (2022) 120789, https://doi.org/10.1016/j.seppur.2022.120789.
[28] Y. Yang, X. Meng, H. Cao, X. Lin, C. Liu, Y. Sun, Y. Zhang, Z. Sun, Selective recovery of lithium from spent lithium iron phosphate batteries: a sustainable process, Green Chem. 20 (2018) 3121–3133, https://doi.org/10.1039/C7GC03376A.
[29] R. Reich, K. Slunitschek, R.M. Danisi, E. Eiche, J. Kolb, Lithium extraction techniques and the application potential of different sorbents for Lithium recovery from brines, Miner. Process. Extr. Metall. Rev. (2022) 1–20, https://doi.org/10.1080/08827508.2022.2047041.
[30] JCPDS-ICDD, PDF-2 Release 2002, In, ICDD, Newton Square, Pennsylvania, USA, 2002.
[31] H.N. Tran, S.-J. You, A. Hosseini-Bandegharaei, H.-P. Chao, Mistakes and inconsistencies regarding adsorption of contaminants from aqueous solutions: a critical review, Water Res. 120 (2017) 88–116, https://doi.org/10.1016/j.watres.2017.04.014.
[32] R. Reich, R.M. Danisi, T. Kluge, E. Eiche, J. Kolb, Structural and compositional variation of zeolite 13X in lithium sorption experiments using synthetic solutions and geothermal brine, Microporous Mesoporous Mater. 359 (2023) 112623, https://doi.org/10.1016/j.micromeso.2023.112623.
[33] E. Muneyama, A. Kunishige, K. Ohdan, M. Ai, Reduction and reoxidation of iron phosphate and its catalytic activity for oxidative dehydrogenation of isobutyric acid, J. Catal. 158 (1996) 378–384, https://doi.org/10.1006/jcat.1996.0039.
[34] M.T. Paques-Ledent, P. Tarte, Vibrational studies of olivine-type compounds—II orthophosphates,-arsenates and-vanadates AIBIIXVO4, Spectrochim. Acta A: Mol. Spectrosc. 30 (1974) 673–689, https://doi.org/10.1016/0584-8539(74)80190-X.
[35] C.M. Burba, R. Frech, In situ transmission FTIR spectroelectrochemistry: a new technique for studying lithium batteries, Electrochim. Acta 52 (2006) 780–785, https://doi.org/10.1016/j.electacta.2006.06.007.
[36] A. Ait-Salah, J. Dodd, A. Mauger, R. Yazami, F. Gendron, C. Julien, Structural and magnetic properties of LiFePO4 and lithium extraction effects, Z. Anorg. Allg. Chem. 632 (2006) 1598–1605, https://doi.org/10.1002/zaac.200600090.
[37] N. Rajić, R. Gabrovšek, V. Kaučič, Thermal investigation of two FePO materials prepared in the presence of 1, 2-diaminoethane, Thermochim. Acta 359 (2000) 119–122, https://doi.org/10.1016/S0040-6031(00)00512-8.
[38] F. Faure, N. Arndt, G. Libourel, Formation of spinifex texture in komatiites: an experimental study, J. Petrol. 47 (2006) 1591–1610, https://doi.org/10.1093/petrology/egl021.

[39] R. Miyawaki, F. Hatert, M. Pasero, S.J. Mills, IMA Commission on new minerals, nomenclature and classification (CNMNC) – newsletter 67, Eur. J. Mineral. 34 (2022) 359–364, https://doi.org/10.5194/ejm-34-359-2022.
[40] R. Miyawaki, F. Hatert, M. Pasero, S.J. Mills, IMA Commission on new minerals, nomenclature and classification (CNMNC) – newsletter 62, Eur. J. Mineral. 33 (2021) 479–484, https://doi.org/10.5194/ejm-33-479-2021.
[41] J. Lemaire, L. Svecova, F. Lagallarde, R. Laucournet, P.-X. Thivel, Lithium recovery from aqueous solution by sorption/desorption, Hydrometallurgy 143 (2014) 1–11, https://doi.org/10.1016/j.hydromet.2013.11.006.
[42] G. Limousin, J.-P. Gaudet, L. Charlet, S. Szenknect, V. Barthes, M. Krimissa, Sorption isotherms: a review on physical bases, modeling and measurement, Appl. Geochem. 22 (2007) 249–275, https://doi.org/10.1016/j.apgeochem.2006.09.010.
[43] Y.O. Rosenberg, I.J. Reznik, S. Zmora-Nahum, J. Ganor, The effect of pH on the formation of a gypsum scale in the presence of a phosphonate antiscalant, Desalination 284 (2012) 207–220, https://doi.org/10.1016/j.desal.2011.08.061.
[44] J. Alonso-Azcárate, S. Bottrell, J. Tritlla, Sulfur redox reactions and formation of native sulfur veins during low grade metamorphism of gypsum evaporites, Cameros Basin (NE Spain), Chem. Geol. 174 (2001) 389–402, https://doi.org/10.1016/S0009-2541(00)00286-2.
[45] A.F. Holleman, N. Wiberg, Grundlagen und Hauptgruppenelemente, Walter de Gruyter GmbH & Co KG, 2016.
[46] L. Chang, R. Howie, J. Zussman, Rock-Forming Minerals, Volume 5B, Non-Silicates, Sulphates, Carbonates, Phosphates and Halides. Second Edition, The Geological Society, London, 1996.
[47] E. Walker, The functional group selectivity of complex hydride reducing agents, Chem. Soc. Rev. 5 (1976) 23–50, https://doi.org/10.1039/CS9760500023.
[48] B.G. Ruiz, S. Roux, F. Courtois, C. Bonazzi, Kinetic modelling of ascorbic and dehydroascorbic acids concentrations in a model solution at different temperatures and oxygen contents, Food Res. Int. 106 (2018) 901–908, https://doi.org/10.1016/j.foodres.2018.01.051.
[49] E. Kimoto, H. Tanaka, T. Ohmoto, M. Choami, Analysis of the transformation products of dehydro-L-ascorbic acid by ion-pairing high-performance liquid chromatography, Anal. Biochem. 214 (1993) 38–44, https://doi.org/10.1006/abio.1993.1453.
[50] J.-P. Yuan, F. Chen, Degradation of ascorbic acid in aqueous solution, J. Agric. Food Chem. 46 (1998) 5078–5082, https://doi.org/10.1021/jf9805404.
[51] IFA, GESTIS-Substance Database: 2-Furaldehyde, (2024) https://gestis.dguv.de/data?name=025010&lang=en (11.04.2024).
[52] ThermoFisher Scientific, Sicherheitsdatenblatt gemäß Verordnung (EG) Nr. 1907/2006: Brenzschleimsaeure, (2023) https://www.fishersci.ch/store/msds?partNumber=10309323&countryCode=CH&language=de (11.04.2024).
[53] R. Fuge, C.C. Johnson, Iodine and human health, the role of environmental geochemistry and diet, a review, Appl. Geochem. 63 (2015) 282–302, https://doi.org/10.1016/j.apgeochem.2015.09.013.
[54] S.A. Patil, R.R. Rodriguez-Berrios, D. Chavez-Flores, D.V. Wagle, A. Bugarin, Recent advances in the removal of radioactive iodine and iodide from the environment, ACS ES&T Water 3 (2023) 2009–2023, https://doi.org/10.1021/acsestwater.3c00111.
[55] P. Yao, H. Zhao, M. Zhang, C. Xia, T. Yang, Q. Li, Synthesis of α-AlH3 by organic liquid reduction method and its hydrogen desorption performance, Int. J. Hydrogen Energy (2023), https://doi.org/10.1016/j.ijhydene.2023.05.170.